molecules

MDPI

Article

# Identification of Antibacterial Components in the Methanol-Phase Extract from Edible Herbaceous Plant *Rumex madaio* Makino and Their Antibacterial Action Modes

**Yue Liu [1], Lianzhi Yang [1], Pingping Liu [1], Yinzhe Jin [1], Si Qin [2,*] and Lanming Chen [1,*]**

[1] Key Laboratory of Quality and Safety Risk Assessment for Aquatic Products on Storage and Preservation (Shanghai), Ministry of Agriculture and Rural Affairs of the People's Republic of China, College of Food Science and Technology, Shanghai Ocean University, Shanghai 201306, China; M190300758@st.shou.edu.cn (Y.L.); D210300069@st.shou.edu.cn (L.Y.); ppliu@shou.edu.cn (P.L.); yzjin@shou.edu.cn (Y.J.)

[2] Key Laboratory for Food Science and Biotechnology of Hunan Province, College of Food Science and Technology, Hunan Agricultural University, Changsha 410128, China

* Correspondence: qinsiman@hunau.edu.cn (S.Q.); lmchen@shou.edu.cn (L.C.)

**Abstract:** Outbreaks and prevalence of infectious diseases worldwide are some of the major contributors to morbidity and morbidity in humans. Pharmacophageous plants are the best source for searching antibacterial compounds with low toxicity to humans. In this study, we identified, for the first time, antibacterial components and action modes of methanol-phase extract from such one edible herbaceous plant *Rumex madaio* Makino. The bacteriostatic rate of the extract was 75% against 23 species of common pathogenic bacteria. The extract was further purified using the preparative high-performance liquid chromatography (Prep-HPLC) technique, and five separated componential complexes (CC) were obtained. Among these, the CC 1 significantly increased cell surface hydrophobicity and membrane permeability and decreased membrane fluidity, which damaged cell structure integrity of Gram-positive and -negative pathogens tested. A total of 58 different compounds in the extract were identified using ultra-HPLC and mass spectrometry (UHPLC-MS) techniques. Comparative transcriptomic analyses revealed a number of differentially expressed genes and various changed metabolic pathways mediated by the CC1 action, such as down-regulated carbohydrate transport and/or utilization and energy metabolism in four pathogenic strains tested. Overall, the results in this study demonstrated that the CC1 from *R. madaio* Makino are promising candidates for antibacterial medicine and human health care products.

**Keywords:** *Rumex madaio* Makino; antibacterial component; antibacterial mode; pathogenic bacteria; transcriptome; edible plant

check for updates

**Citation:** Liu, Y.; Yang, L.; Liu, P.; Jin, Y.; Qin, S.; Chen, L. Identification of Antibacterial Components in the Methanol-Phase Extract from Edible Herbaceous Plant *Rumex madaio* Makino and Their Antibacterial Action Modes. *Molecules* **2022**, *27*, 660. https://doi.org/10.3390/molecules27030660

Academic Editor: Hristo Najdenski

Received: 24 November 2021
Accepted: 12 January 2022
Published: 20 January 2022



## 1. Introduction

China is one of the richest countries in biodiversity, with very high levels of plant endemism [1]. Pharmacopoeia of the Peoples' Republic of China (2020 Edition) contains 2711 species of Chinese herbal plants, which constitute a gold mine for exploiting medicine candidates and health care products [2]. For instance, *R. madaio* Makino is an edible, perennial and herbaceous plant that belongs to the *Dicotyledoneae* class, *Polygonaceae* family, and *Rumex* genus. According to the National Compilation of Chinese Herbal Medicine (1996 Edition), leaf and root tissues of *R. madaio* Makino can be used as medicine such as clearing heat and detoxification, removing blood stasis, and defecating and killing insects. Nevertheless, current studies on the antibacterial activity of *R. madaio* Makino are rare.

In this study, antibacterial components and action modes of methanol-phase extract from *R. madaio* Makino were for the first time identified. The objectives of this study were: (1) to extract bioactive substances from *R. madaio* Makino using the methanol and chloroform extraction (MCE) method, and determine their inhibition activity against 23 species

of pathogenic bacteria; (2) to purify the methanol-phase extract from *R. madaio* Makino by preparation high-performance liquid chromatography (Prep-HPLC) analysis, and identify bioactive compounds in componential complex 1 (CC 1) using an ultra-HPLC and mass spectrometry (UHPLC-MS) technique; (3) to determine cell surface hydrophobicity, cell membrane permeability, fluidity, and the damage of four representative pathogenic strains treated with the CC 1; (4) to decipher possible molecular mechanisms underlying antibacterial activity by comparative transcriptomic analysis. The results of this study meet the increasing need for novel antibacterial agent candidates against common pathogenic bacteria.

## 2. Results and Discussion

### *2.1. Antibacterial Activity of Crude Extracts from R. madaio Makino*

Antibacterial substances in fresh leaf and stem tissues of *R. madaio* Makino were extracted using the MCE method. The results showed that the water loss rate of the plant material was 93.32%, and extraction rates of the methanol phase and chloroform phase were 32.10% and 29.60%, respectively. Antibacterial activity of the crude extracts against 23 species of pathogenic bacteria was determined, most of which are common foodborne pathogens, and the results are presented in Table 1. The chloroform-phase crude extract from *R. madaio* Makino showed a bacteriostatic rate of 39%, inhibiting 2 species of Gram-positive and 11 species of Gram-negative pathogens (Table 1, Figure 1). Remarkably, the methanol-phase crude extract from *R. madaio* Makino inhibited the growth of 33 bacteria strains tested with a bacteriostatic rate of 75%, including 2 species of Gram-positive and 18 species of Gram-negative pathogens (Table 1). Based on the higher bacteriostatic rate (75%), the methanol-phase crude extract from *R. madaio* Makino was chosen for further analysis in this study.

**Table 1.** Antibacterial activity of crude extracts from *R. madaio* Makino.

| pStrain | Inhibition Zone (Diameter, mm) | | MIC (μg/mL) | |
|---|---|---|---|---|
| | CPE | MPE | CPE | MPE |
| *Aeromonas hydrophila* ATCC35654 | — | 11.30 ± 0.47 | — | 126 |
| *Bacillus cereus* A1-1 | — | 14.70 ± 1.25 | — | 32 |
| *Enterobacter cloacae* ATCC13047 | 7.90 ± 0.05 | 13.00 ± 0.86 | 512 | 64 |
| *Enterobacter cloacae* | — | 8.30 ± 0.24 | — | 512 |
| *Escherichia coli* ATCC8739 | — | — | — | — |
| *Escherichia coli* ATCC25922 | — | — | — | — |
| *Escherichia coli* K12 | — | 9.30 ± 1.25 | — | 128 |
| *Enterobacter sakazakii* CMCC45401 | 8.90 ± 0.14 | 8.70 ± 0.47 | 256 | 512 |
| *Listeria monocytogenes* ATCC19115 | 9.80 ± 0.17 | — | 256 | — |
| *Pseudomonas aeruginosa* ATCC9027 | — | 9.30 ± 0.94 | — | 256 |
| *Pseudomonas aeruginosa* ATCC27853 | — | 9.00 ± 0.21 | — | 256 |
| *Salmonella choleraesuis* ATCC13312 | — | 9.70 ± 0.94 | — | 256 |
| *Salmonella paratyphi-A* CMCC50093 | 8.70 ± 0.94 | 9.40 ± 0.43 | 512 | 256 |
| *Salmonella typhimurium* ATCC15611 | 8.90 ± 0.17 | 14.00 ± 0.82 | 256 | 32 |
| *Salmonella* | 8.20 ± 0.17 | 20.30 ± 0.47 | 512 | 8 |
| *Shigella dysenteriae* CMCC51252 | — | — | — | — |
| *Shigella flexneri* CMCC51572 | — | 10.00 ± 0.00 | — | 128 |
| *Shigella flexneri* ATCC12022 | — | — | — | — |
| *Shigella flexneri* CMCC51574 | — | — | — | — |
| *Shigella sonnei* ATCC25931 | — | — | — | — |
| *Shigella sonnet* CMCC51592 | 9.40 ± 0.29 | 8.10 ± 0.05 | 256 | 512 |
| *Staphylococcus aureus* ATCC25923 | 10.60 ± 0.42 | 8.10 ± 0.29 | 128 | 512 |
| *Staphylococcus aureus* ATCC8095 | 8.00 ± 0.05 | 7.30 ± 0.21 | 512 | 1024 |
| *Staphylococcus aureus* ATCC29213 | — | 7.20 ± 0.08 | — | 1024 |
| *Staphylococcus aureus* ATCC6538 | 10.00 ± 0.82 | 10.00 ± 2.16 | 256 | 256 |
| *Staphylococcus aureus* ATCC6538P | — | 10.50 ± 0.41 | — | 128 |

**Table 1.** *Cont.*

| pStrain | Inhibition Zone (Diameter, mm) | | MIC (μg/mL) | |
|---|---|---|---|---|
| | CPE | MPE | CPE | MPE |
| *Staphylococcus aureus* | 7.00 ± 0.00 | 8.50 ± 0.41 | 1024 | 512 |
| *Vibrio alginolyticus* ATCC17749 | — | 24.30 ± 1.25 | — | 4 |
| *Vibrio alginolyticus* ATCC33787 | — | — | — | — |
| *Vibrio cholerae* Q10-54 | — | — | — | — |
| *Vibrio cholerae* b10-49 | — | 9.00 ± 0.24 | — | 256 |
| *Vibrio cholerae* GIM1.449 | 10.30 ± 0.36 | 10.50 ± 0.41 | 256 | 128 |
| *Vibrio fluvialis* ATCC33809 | 11.30 ± 0.47 | 7.90 ± 0.09 | 128 | 512 |
| *Vibrio harvey* ATCC BAA-1117 | — | 8.00 ± 0.05 | — | 512 |
| *Vibrio harveyi* ATCC33842 | — | — | — | — |
| *Vibrio metschnikovii* ATCC700040 | 8.40 ± 0.42 | — | 512 | — |
| *Vibrio mimicus* bio-56759 | 9.20 ± 0.12 | 13.00 ± 0.82 | 512 | 64 |
| *Vibrio parahaemolyticus* B3-13 | 10.50 ± 0.41 | 9.10 ± 0.12 | 128 | 256 |
| *Vibrio parahaemolyticus* B4-10 | — | 10.30 ± 0.47 | — | 128 |
| *Vibrio parahaemolyticus* B5-29 | — | 12.30 ± 0.94 | — | 64 |
| *Vibrio parahaemolyticus* B9-35 | — | 8.30 ± 0.21 | — | 512 |
| *Vibrio parahaemolyticus* ATCC17802 | — | 13.70 ± 0.94 | — | 128 |
| *Vibrio parahaemolyticus* ATCC33847 | — | 13.00 ± 0.00 | — | 64 |
| *Vibrio vulnificus* ATCC27562 | 11.70 ± 1.25 | 8.70 ± 0.47 | 128 | 256 |

Note: CPE: chloroform phase extract. MPE: methanol phase extract. —: no bacteriostasis activity. Inhibition zone: diameter includes the disk diameter (6 mm). MIC: minimum inhibitory concentration. Values are means ± S.D. of three parallel measurements.

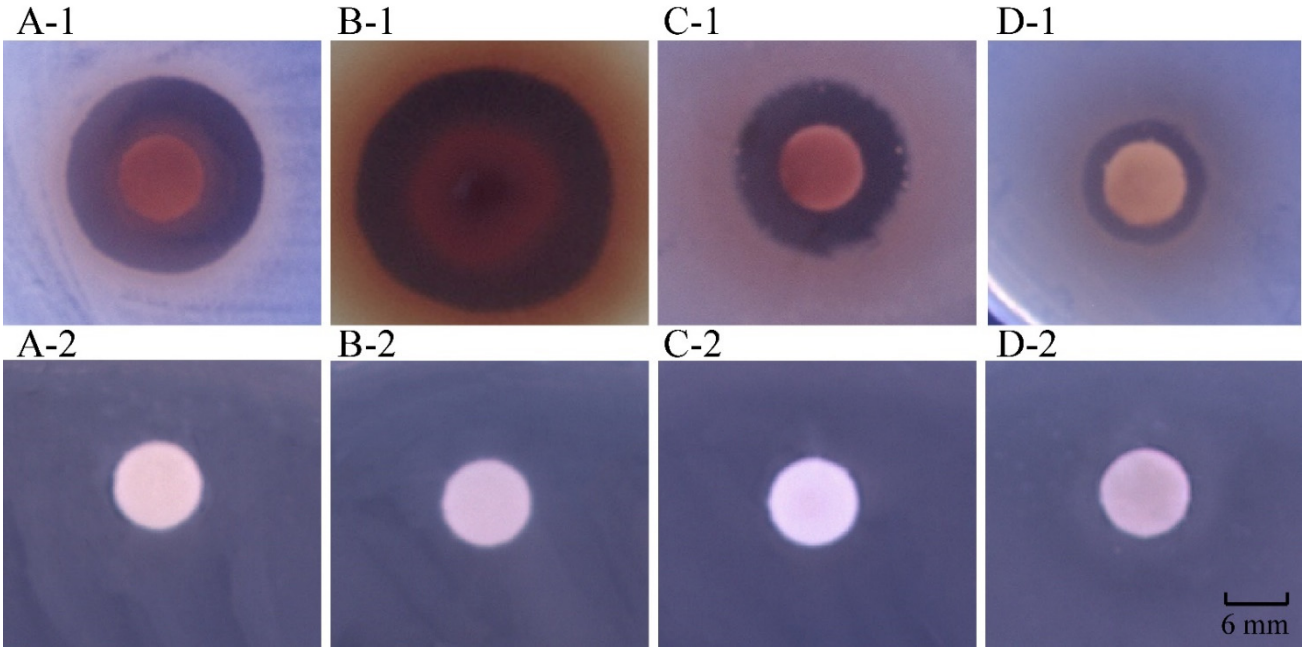


**Figure 1.** Inhibition activity of the methanol-phase crude extract from *R. madaio* Makino against the four representative bacterial strains. (**A-1**): *B. cereus* A1-1; (**B-1**): *V. alginolyticus* ATCC17749; (**C-1**): *V. Parahaemolyticus* ATCC17802; and (**D-1**): *V. Parahaemolyticus* B4-10. (**A-2**–**D-2**): negative control, respectively.

### *2.2. Purification of the Methanol-Phase Crude Extract from R. madaio Makino*

Large amounts of the methanol-phase crude extract from *R. madaio* Makino were further purified by the Prep-HPLC analysis. As shown in Figure 2, five obviously separated peaks (designated as componential complex, CCs 1 to 5) were observed by scanning at $OD_{280\ nm}$ for 15 min.

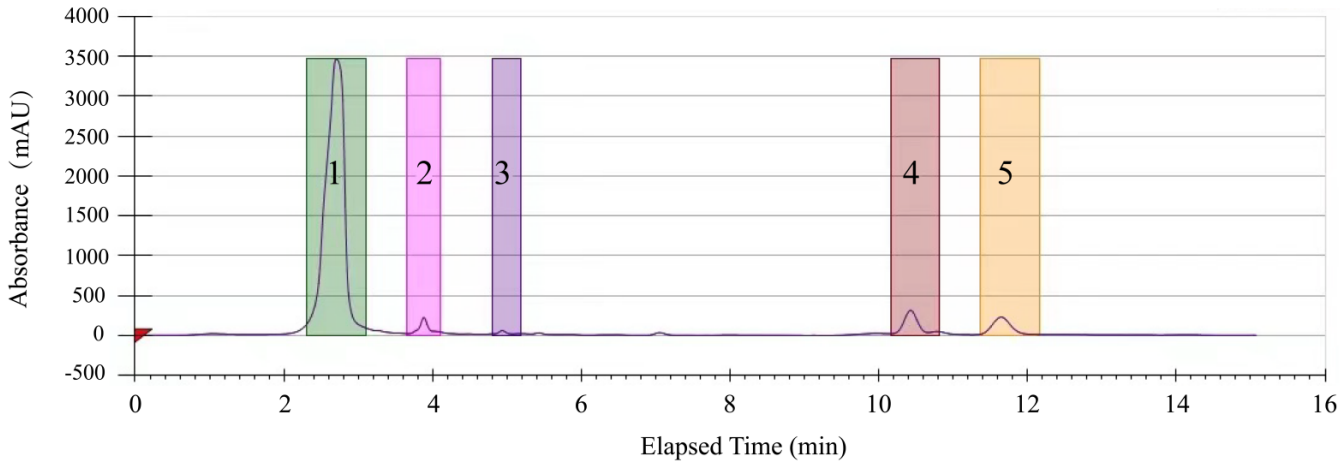


**Figure 2.** The Prep−HPLC diagram of purifying the methanol-phase crude extract from *R. madaio* Makino.

These five single peaks were individually collected for antibacterial activity analysis. The results revealed that the CC 1 had strong inhibitory effects on *Vibrio parahaemolyticus* ATCC17802, *Vibrio alginolyticus* ATCC17749, *Bacillus cereus* A1-1, and *V. parahaemolyticus* B4-10. Moreover, the growth of the other four strains was also depressed, including *V. parahaemolyticus* ATCC33847, *V. parahaemolyticus* B3-13, *V. parahaemolyticus* B5-29, and *Staphylococcus aureus* ATCC6538 (Table 2). Among these, *V. alginolyticus* is an opportunistic pathogenic bacterium that can infect a broad range of marine host animals, including fish, crab and pearl oysters, and can also infect the human ear, soft tissue and wounded sites [3,4], while *V. parahaemolyticus* is a leading seafood-borne pathogen worldwide and can cause acute gastroenteritis and septicemia in humans [5]. *B. cereus* is a Gram-positive bacterium for food poisoning. This bacterium has been incriminated in clinical conditions such as anthrax-like progressive pneumonia, fulminant sepsis, and devastating central nervous system infections, particularly in immunosuppressed individuals, intravenous drug abusers, and neonates [6].

**Table 2.** Antibacterial activity of the CC 1 from *R. madaio* Makino.

| Strain | Inhibition Zone (Diameter, mm) | MIC (μg/mL) |
|---|---|---|
| *B. cereus* A1-1 | 10.30 ± 0.24 | 128 |
| *S. typhimurium* ATCC15611 | 7.90 ± 0.22 | 512 |
| *S. aureus* ATCC6538 | 7.00 ± 0.05 | 1024 |
| *V. alginolyticus* ATCC17749 | 11.20 ± 0.21 | 64 |
| *V. parahaemolyticus* ATCC17802 | 11.10 ± 0.08 | 64 |
| *V. parahaemolyticus* ATCC33847 | 7.90 ± 0.25 | 256 |
| *V. parahaemolyticus* B3-13 | 7.10 ± 0.09 | 512 |
| *V. parahaemolyticus* B4-10 | 9.40 ± 0.26 | 256 |
| *V. parahaemolyticus* B5-29 | 8.10 ± 0.12 | 512 |

Note: MIC: minimum inhibitory concentration.

Conversely, the other four peaks (CCs 2 to 4) showed weak or no antibacterial activity, indicating that bioactive compounds in the methanol-phase extract from *R. madaio* Makino existed in the CC 1.

MIC values of the CC 1 were also determined, which was 64 μg/mL against *V. alginolyticus* ATCC17749 and *V. parahaemolyticus* ATCC17802; 128 μg/mL against *B. cereus* A1-1; and 256 μg/mL against *V. parahaemolyticus* B4-10.

### *2.3. Changed Bacterial Cell Surface Structure by the CC 1 Extract*

To decipher possible mechanisms underlying bacteriostatic activity of the CC 1, the cell structure of the four highly inhibited strains were observed by the transmission electron microscope (TEM) analysis. As shown in Figure 3, in remarkable contrast to control

groups whose cell surface structure was intact, showing rod cells, a flat surface, and a clear structure, bacterial cells in the treatment groups showed different degrees of contraction and rupture, some of which were deformed with obvious depressions, folds or cavities on the surface. For example, for the Gram-positive *B. cereus* A1-1, the 2 h treatment by the CC 1 resulted in the bacterial cell surface shrinking seriously, the flagella breaking, and some contents leaking. After being treated for 4 h, cell surface shrinkage was intensified, and more cells were ruptured. After being treated for 6 h, the cell structure was seriously damaged, a large number of contents exuded, and only a few cells still maintained rod shape (Figure 3A). For the Gram-negative *V. parahaemolyticus* ATCC17802, after being treated with the CC 1 for 2 h, its cell surface shrunk slightly, and pili structure was still visible. However, after being treated for 4 h, the cell surface shrinkage increased and the cell membrane folded. *V. parahaemolyticus* ATCC17802 cells were destroyed, seriously shrunk and deformed after being treated for 6 h (Figure 3C). These results indicated that the CC 1 from *R. madaio* Makino damaged the cell surface structure of the Gram-negative and Gram-positive pathogens.

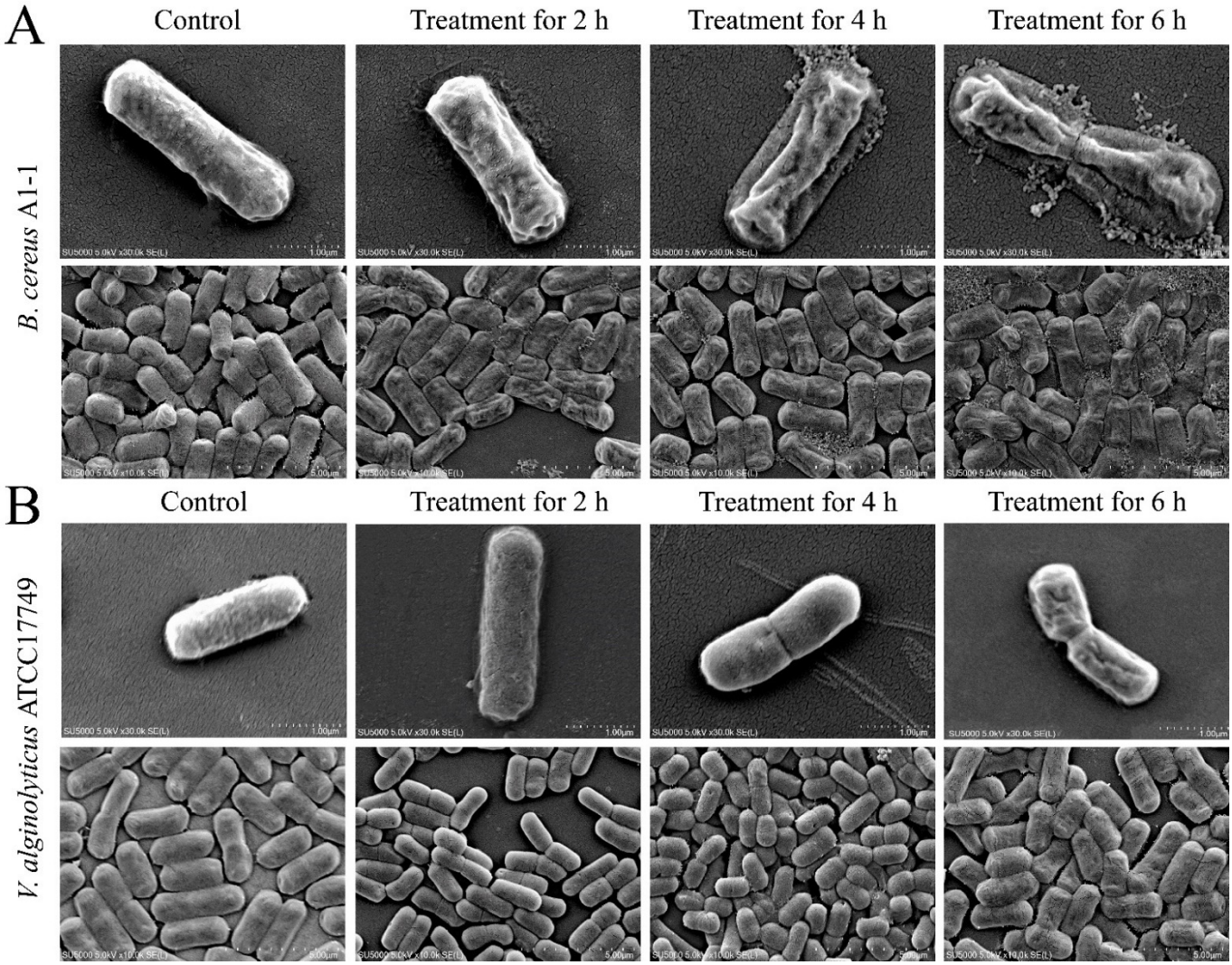


**Figure 3.** *Cont.*

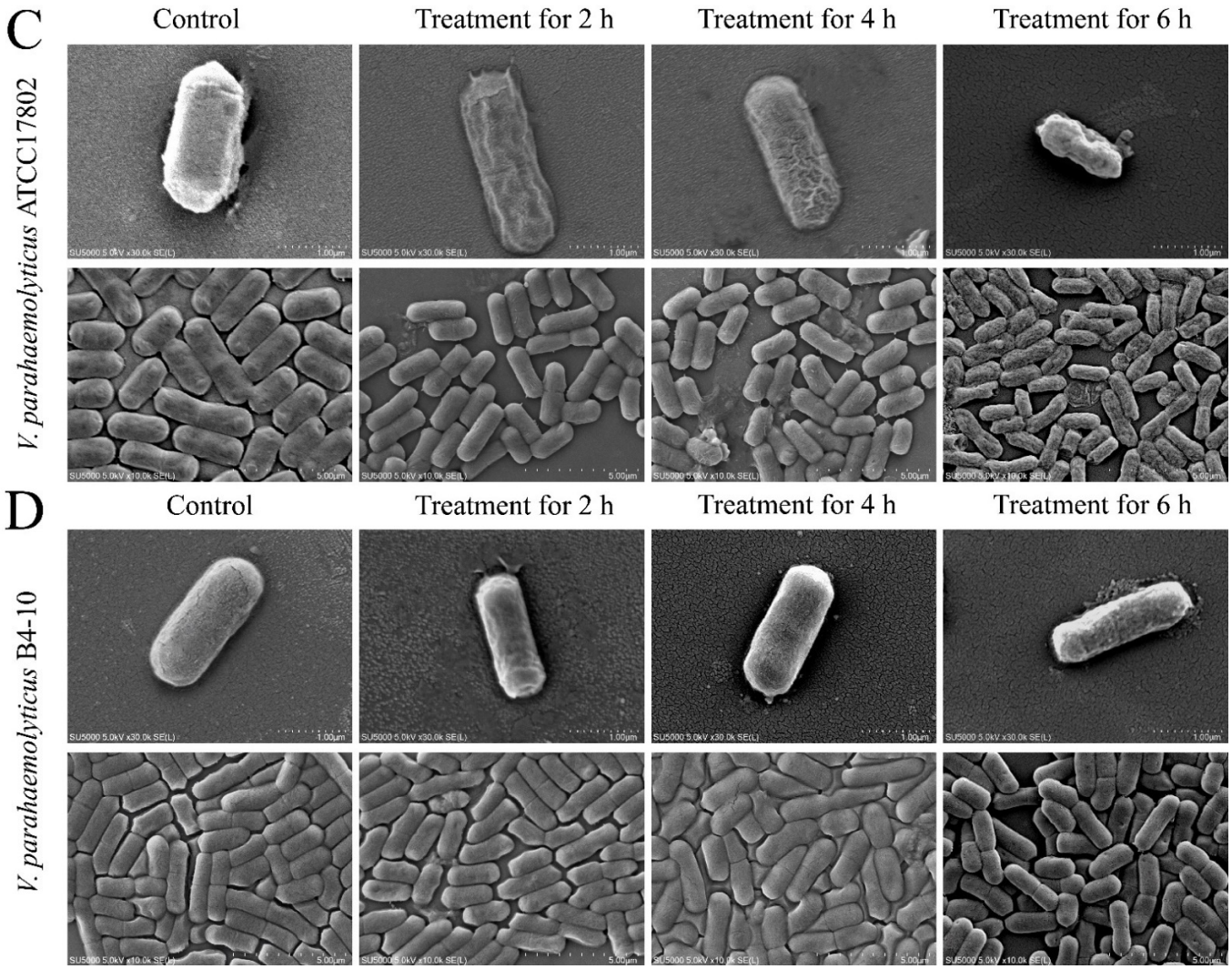


**Figure 3.** The TEM observation of cell surface structure of the four bacterial strains treated with the CC1 for different times. (**A**): *B. cereus* A1-1; (**B**): *V. alginolyticus* ATCC17749; (**C**): *V. Parahaemolyticus* ATCC17802; and (**D**): *V. Parahaemolyticus* B4-10.

### *2.4. Changed Bacterial Cell Surface Hydrophobicity, Cell Membrane Fluidity, Permeability, and Damage by the CC 1 from R. madaio Makino*

Cell surface hydrophobicity plays an important role in the adhesion to abiotic and biological surfaces and infiltration of host tissue [7]. In this study, bacterial cell surface hydrophobicity of all four experimental groups was significantly increased ($p < 0.05$) when compared with the control groups (Figure 4A). The effect was highly enhanced with the increase in treatment time. For example, cell surface hydrophobicity was significantly increased in *V. parahaemolyticus* ATCC17802 (1.47-fold), *V. parahaemolyticus* B4-10 (1.62-fold) and *B. cereus* A1-1 (1.42-fold) after being treated with the CC1 for 2 h ($p < 0.05$), whereas a similar change was observed in the treatment group of *V. alginolyticus* ATCC17749 (1.48-fold) after being treated for 4 h. Moreover, the highest increase in cell surface hydrophobicity was observed in *B. cereus* A1-1 (3.75-fold) after being treated with the CC1 for 6 h (Figure 4A).

Membrane fluidity is also a key parameter of the bacterial cell membrane that undergoes quick adaptation in response to environmental challenges [8]. It has recently been regarded as an important factor in the antibacterial mechanism of membrane-targeting antibiotics [9]. In this study, compared with the control groups, there was no significant difference in cell membrane fluidity of *V. parahaemolyticus* ATCC17802 and B4-10, as well as *V. alginolyticus* ATCC17749 after being treated with the CC 1 for 2 h ($p > 0.05$). However,

a significant decrease in membrane fluidity of these three strains was observed after the treatment for 4 h. Additionally, cell membrane fluidity significantly declined in *B. cereus* A1-1 (1.20-fold) treated with the CC 1 for 2 h, and sharply lost for 6 h (8.11-fold) (Figure 4B). The change of membrane lipid composition likely contributed to the observed membrane fluidity change to resist the lipid disorder effect by therapeutic agents [10].

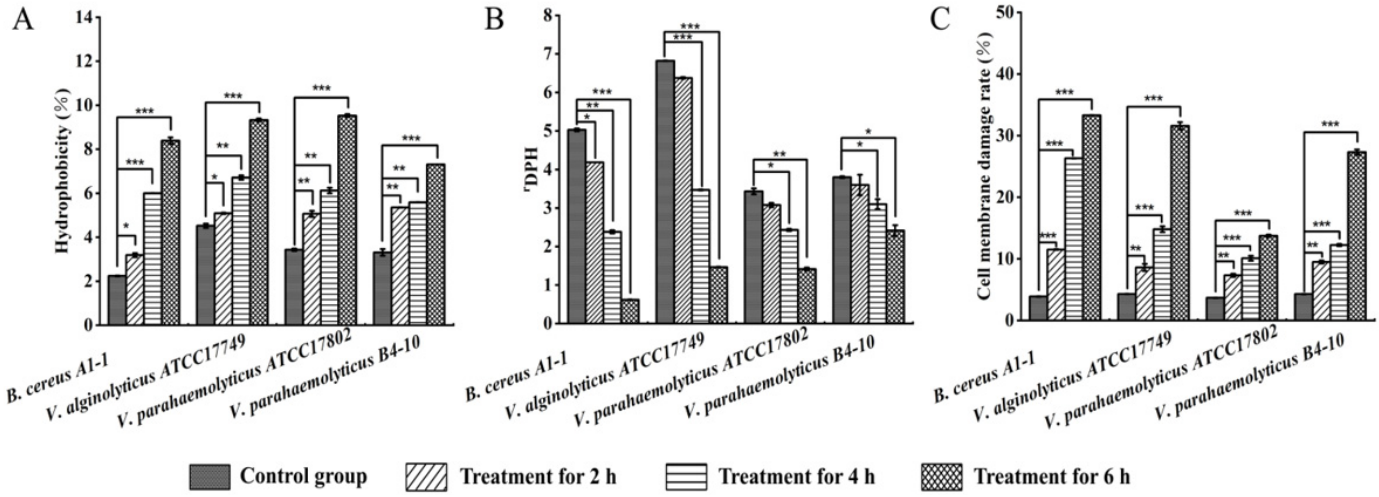


**Figure 4.** Effects of the CC 1 from *R. madaio* Makino on cell surface hydrophobicity, membrane fluidity and damage of the four bacterial strains. (**A**): cell surface hydrophobicity; (**B**): cell membrane fluidity; and (**C**): cell membrane damage. The results were represented as the mean ± standard deviation of three repetitions. *: $p < 0.05$; **: $p < 0.01$; and ***: $p < 0.001$.

The o-nitrophenyl-β-D-galactopyranoside (o-nitrophenyl)-β-D-galactopyranoside (ONPG) was used as a probe to monitor the inner cell membrane permeability of the four bacterial strains, and the results were illustrated in Figure 5. Different influence of the CC 1 from *R. madaio* Makino on inner cell membrane permeability was observed among the four treatment groups. For example, *V. alginolyticus* ATCC17749 did not change significantly in the inner cell membrane permeability after the treatment for 2 h ($p > 0.05$), whereas a significant increase was observed after being treated for 4 h (1.15-fold) and 6 h (1.18-fold), respectively ($p < 0.05$) (Figure 5).

*N*-Phenyl-1-naphthylamine (NPN) was used as a probe to monitor the bacterial outer membrane permeability. As shown in Figure 6, the outer membrane permeability in the four experimental groups were all highly increased after the treatment with the CC 1 for 2 h ($p < 0.01$). The highest increase was found in *B. cereus* A1-1 (6.06-fold) after being treated for 6 h, whereas an opposite pattern was observed in *V. parahaemolyticus* ATCC17802 (1.77-fold).

As shown in Figure 4C, when compared with the control groups, cell membrane damage rates of all four experimental groups significantly increased ($p < 0.05$), which raised with the increase in treatment time. Significant damage was observed in *B. cereus* A1-1 (2.95-fold) and *V. parahaemolyticus* B4-10 (2.21-fold) after being treated for 2 h, whereas a similar change was found in the other two strains treated for 4 h. Moreover, cell membrane damage of *B. cereus* A1-1 was the most severe among the four strains after being treated for 6 h (8.54-fold).

Taken together, these results demonstrated that the CC 1 from *R. madaio* Makino significantly increased bacterial cell surface hydrophobicity and membrane permeability and decreased membrane fluidity of *V. parahaemolyticus* ATCC17802, *V. parahaemolyticus* B4-10, *V. alginolyticus* ATCC17749, and *B. cereus* A1-1, consistent with the observed bacterial surface structure by the TEM analysis. The damaged cell surface and membrane structure integrity were beneficial for the CC1 to penetrate bacterial cell envelope to target intracellular processes.

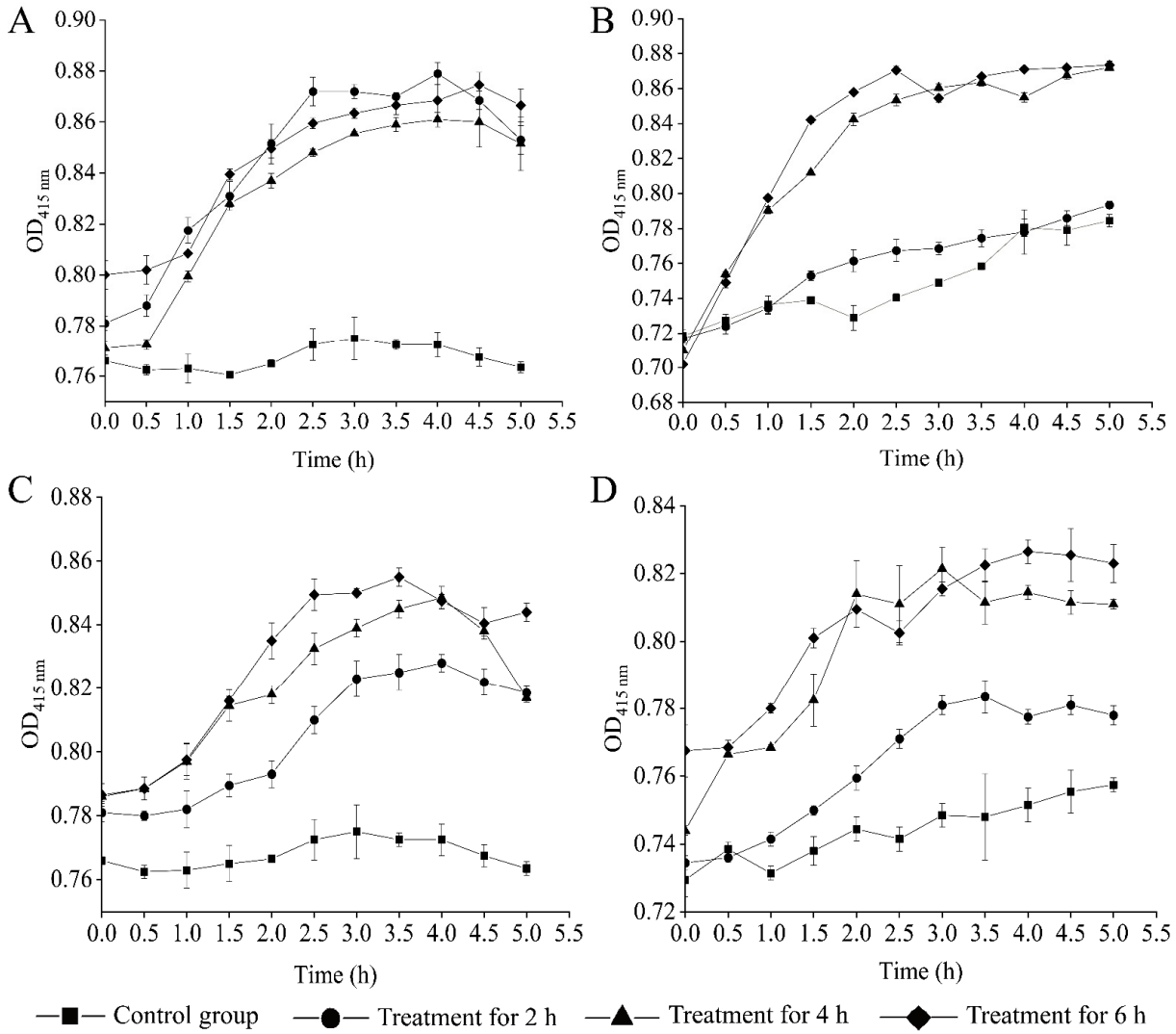


**Figure 5.** Effects of the CC 1 from *R. madaio* Makino on inner cell membrane permeability of the four bacterial strains. (**A**): *B. cereus* A1-1; (**B**): *V. alginolyticus* ATCC17749; (**C**): *V. Parahaemolyticus* ATCC17802; and (**D**): *V. Parahaemolyticus* B4-10.

### *2.5. Identification of Potential Antibacterial Compounds in the CC 1 from R. madaio Makino*

The obtained CC 1 resolved in $H_2O$ was subjected to UHPLC-MS analysis. As shown in Table 3, a total of 58 different compounds were identified. The highest percentage of these compounds in the CC 1 was p-phenol ethanolamine (18.62%), followed by D-2-aminobutyric acid (9.46%), sucrose (7.01%), turanose (7.01%), and lactulose (7.01%). Some compounds with lower concentrations were also identified from the extract (0.83–0.07%), including a galactose 1-phosphate, L-glutamic acid, and kojibiose (Table 3). Phenols and organic acids have good antioxidant and antibacterial activities [11], while alkaloids can inhibit the formation of and/or disperse bacterial biofilms [12]. For example, the indole of alkaloids is a versatile heterocyclic compound with various pharmacological activities such as anticancer, anticonvulsant, antimicrobial, antitubercular, antimalarial, antiviral, antidiabetic and other miscellaneous activities. Indole also regulates various aspects of bacterial physiology, including spore formation, plasmid stability, resistance to drugs, biofilm formation and virulence [13]. Saccharides have been used to preserve foods for a long history by changing cell osmolarity to inhibit harmful bacterial growth. Kojibiose is a natural disaccharide comprising two glucose moieties linked by an α-1,2 glycosidic bond. It has been reported that Kojibiose can inhibit bacterial proliferation and have anti-inflammatory and antiviral activities [14,15]. In contrast, the certain content of the

identified amino acids may not contribute to the observed antibacterial activity by the CC 1 from *R. madaio* Makino.

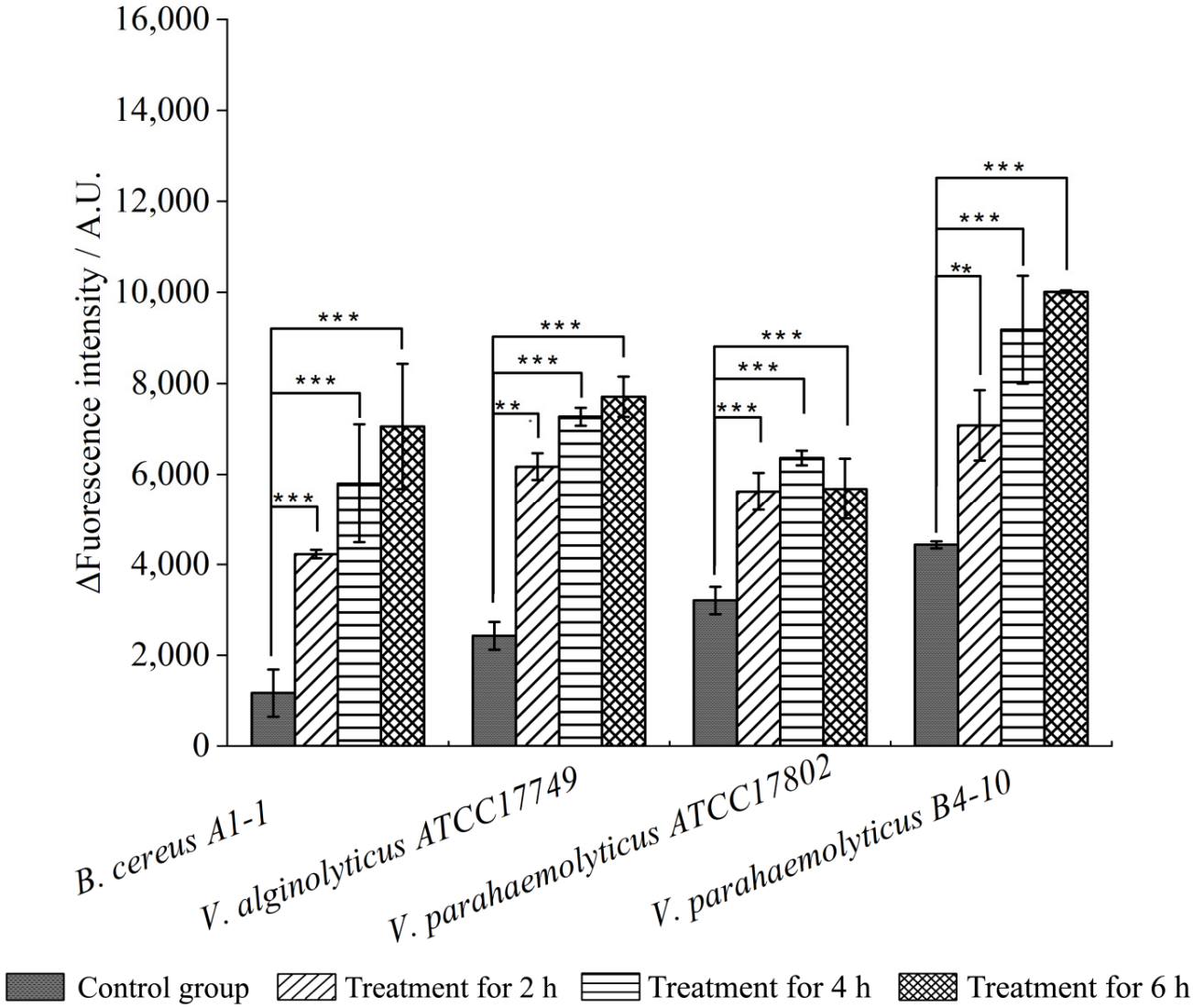


**Figure 6.** Effects of the CC 1 from *R. madaio* Makino on outer cell membrane permeability of the four bacterial strains. The results were represented as the mean ± standard deviation of three repetitions. **: $p < 0.01$; ***: $p < 0.001$.

**Table 3.** Compounds identified in the CC 1 from *R. madaio* Makino by the UHPLC–MS analysis.

| Peak No. | Identified Compound | Compound Nature | Rt (min) | Formula | Exact Mass | Peak Area (%) |
|---|---|---|---|---|---|---|
| 1 | *p*-Octopamine | Biogenic amine | 3.84 | $C_8H_{11}NO_2$ | 153.08 | 18.62 |
| 2 | D-alpha-Aminobutyric acid | Amino acids and derivatives | 0.65 | $C_4H_9NO_2$ | 103.06 | 9.46 |
| 3 | Sucrose | Carbohydrates | 0.89 | $C_{12}H_{22}O_{11}$ | 342.12 | 7.01 |
| 4 | Turanose | Carbohydrates | 0.79 | $C_{12}H_{22}O_{11}$ | 342.12 | 7.01 |
| 5 | Lactulose | Organooxygen compounds | 0.77 | $C_{12}H_{22}O_{11}$ | 342.12 | 7.01 |
| 6 | L-Arginine | Amino acids and derivatives | 0.60 | $C_6H_{14}N_4O_2$ | 174.11 | 4.98 |
| 7 | L-Lysine; L-Glutamine | Amino acids and derivatives | 0.64 | $C_6H_{14}N_2O_2$ | 146.11 | 4.68 |
| 8 | D-Glutamine | Amino acids and derivatives | 0.66 | $C_5H_{10}N_2O_3$ | 146.07 | 4.68 |
| 9 | (2*E*)-Decenoyl-ACP | Carboxylic acids and derivatives | 1.47 | $C_6H_{11}NO_2$ | 129.08 | 3.14 |
| 10 | O-Acetylethanolamine | Alkaloids | 0.67 | $C_4H_9NO_2$ | 103.06 | 3.00 |
| 11 | L-Pipecolic acid | Amino acids and derivatives | 0.69 | $C_6H_{11}NO_2$ | 129.08 | 2.48 |
| 12 | Pyrrolidonecarboxylic acid | Amino acids and derivatives | 0.67 | $C_5H_7NO_3$ | 129.04 | 2.48 |
| 13 | D-Maltose | Carbohydrates | 0.76 | $C_{12}H_{22}O_{11}$ | 342.12 | 1.86 |

**Table 3.** *Cont.*

| Peak No. | Identified Compound | Compound Nature | Rt (min) | Formula | Exact Mass | Peak Area (%) |
|---|---|---|---|---|---|---|
| 14 | Trigonelline | Alkaloids | 0.82 | $C_7H_7NO_2$ | 137.05 | 1.74 |
| 15 | Indole | Alkaloids | 3.82 | $C_8H_7N$ | 117.06 | 1.66 |
| 16 | Uridine 5′-diphospho-D-glucose | Carbohydrates | 0.71 | $C_{15}H_{24}N_2O_{17}P_2$ | 566.06 | 1.65 |
| 17 | Proline; L-Proline | Amino acids and derivatives; | 0.73 | $C_5H_9NO_2$ | 115.06 | 1.53 |
| 18 | D-Proline | Amino acids and derivatives | 0.76 | $C_5H_9NO_2$ | 115.06 | 1.53 |
| 19 | Lubiprostone | Fatty acyls | 12.75 | $C_{20}H_{32}F_2O_5$ | 390.22 | 1.40 |
| 20 | Phosphoric acid | Inganic acids | 0.65 | $H_3O_4P$ | 97.98 | 1.29 |
| 21 | Sarracine | Alkaloids | 13.14 | $C_{18}H_{27}NO_5$ | 337.19 | 0.83 |
| 22 | Galactose 1-phosphate | Organooxygen compounds | 0.65 | $C_6H_{13}O_9P$ | 260.03 | 0.75 |
| 23 | L-Glutamic acid | Amino acids and derivatives | 0.66 | $C_5H_9NO_4$ | 147.05 | 0.67 |
| 24 | Kojibiose | Carbohydrates | 0.72 | $C_{12}H_{22}O_{11}$ | 342.12 | 0.50 |
| 25 | Glucose 6-phosphate | Carbohydrates | 0.65 | $C_6H_{13}O_9P$ | 260.03 | 0.49 |
| 26 | *p*-Aminobenzoate | Benzoic acid derivatives | 0.74 | $C_7H_7NO_2$ | 137.05 | 0.47 |
| 27 | Betaine | Alkaloids | 1.06 | $C_5H_{11}NO_2$ | 117.08 | 0.47 |
| 28 | L-Histidine | Amino acids and derivatives | 0.59 | $C_6H_9N_3O_2$ | 155.07 | 0.44 |
| 29 | 8,9-DiHETrE | Fatty Acyls | 13.03 | $C_{20}H_{34}O_4$ | 338.25 | 0.43 |
| 30 | Gluconic acid | Organic acids | 0.69 | $C_6H_{12}O_7$ | 196.06 | 0.43 |
| 31 | *N*,*N*-Dimethylglycine | Amino acids and derivatives | 1.04 | $C_4H_9NO_2$ | 103.05 | 0.40 |
| 32 | 2-Aminoisobutyric acid | Amino acids and derivatives | 0.98 | $C_4H_9NO_2$ | 103.06 | 0.37 |
| 33 | Diallyl disulfide | Organic disulfide | 0.68 | $C_6H_{10}S_2$ | 146.02 | 0.37 |
| 34 | 2-Hydroxybutanoic acid | Organic acids | 0.64 | $C_4H_8O_3$ | 104.05 | 0.35 |
| 35 | Beta-Sitosterol | Steroids | 12.93 | $C_{29}H_{50}O$ | 414.39 | 0.33 |
| 36 | Phosphorylcholine | Cholines | 0.67 | $C_5H_{14}NO_4P$ | 183.07 | 0.31 |
| 37 | Campesterol | Steroids and steroid derivatives | 12.18 | $C_{28}H_{48}O$ | 400.37 | 0.31 |
| 38 | Gemcitabine | Pyrimidine nucleosides | 0.75 | $C_9H_{11}F_2N_3O_4$ | 263.07 | 0.30 |
| 39 | L-Threonine | Amino acids and derivatives | 0.64 | $C_4H_9NO_3$ | 119.06 | 0.29 |
| 40 | L-Homoserine | Amino acids and derivatives | 0.67 | $C_4H_9NO_3$ | 119.05 | 0.29 |
| 41 | 3-Ethyl-1,2-benzenediol | Phenols | 0.74 | $C_8H_{10}O_2$ | 138.07 | 0.29 |
| 42 | Diacylglycerol | Glycerolipids | 13.42 | $C_{37}H_{70}O_5$ | 568.51 | 0.28 |
| 43 | Rutin | Flavonoids | 5.85 | $C_{27}H_{30}O_{16}$ | 610.15 | 0.27 |
| 44 | cis-Aconitic acid | Organic acids and derivatives | 1.46 | $C_6H_6O_6$ | 174.02 | 0.25 |
| 45 | L-Citruline | Amino acids and derivatives | 0.66 | $C_6H_{13}N_3O_3$ | 175.09 | 0.25 |
| 46 | Wighteone | Flavonoids | 13.01 | $C_{20}H_{18}O_5$ | 338.11 | 0.24 |
| 47 | Beta-D-Fructose 2-phosphate | Carbohydrates | 0.75 | $C_6H_{13}O_9P$ | 260.03 | 0.22 |
| 48 | Maltol | Flavonoids | 0.90 | $C_6H_6O_3$ | 126.03 | 0.21 |
| 49 | Itaconic acid | Organic acids | 0.52 | $C_5H_6O_4$ | 130.03 | 0.21 |
| 50 | Safrole | Benzodioxoles | 12.26 | $C_{10}H_{10}O_2$ | 162.07 | 0.20 |
| 51 | 22-Dehydroclerosterol | Steroids | 12.59 | $C_{29}H_{46}O$ | 410.35 | 0.18 |
| 52 | 8-Hydroxybergapten | Coumarins | 10.56 | $C_{12}H_8O_5$ | 232.04 | 0.17 |
| 53 | Isoquercitrin | Flavonoids | 6.06 | $C_{21}H_{20}O_{12}$ | 464.10 | 0.14 |
| 54 | Miltirone | Diterpenoids | 12.98 | $C_{19}H_{22}O_2$ | 282.16 | 0.11 |
| 55 | Puerarin | Flavonoids | 4.89 | $C_{21}H_{20}O_9$ | 416.11 | 0.11 |
| 56 | Cinchonine | Alkaloids | 11.99 | $C_{19}H_{22}N_2O$ | 294.17 | 0.09 |
| 57 | 3-Ethoxy-4-hydroxybenzaldehyde | Phenols | 5.72 | $C_9H_{10}O_3$ | 166.06 | 0.07 |
| 58 | Lumichrome | Alkaloids | 6.69 | $C_{12}H_{10}N_4O_2$ | 242.08 | 0.07 |

### *2.6. Differential Transcriptomes Mediated by the CC 1 from R. madaio Makino*

To gain insights into the genome-wide gene expression changes mediated by the CC 1 from *R. madaio* Makino, we determined transcriptomes of the four bacterial strains treated for 6 h using Illumina RNA sequencing technology. A complete list of DEGs in the four strains was available in the NCBI SRA database (https://submit.ncbi.nlm.nih.gov/subs/bioproject/, accessed on 17 October 2021) under the accession number PRJNA767551. To validate the transcriptome data, we examined 32 representative DEGs (Table S2) by RT-qPCR analysis, and the resulting data were correlated with those yielded from the transcriptome analysis (Table S2).

#### 2.6.1. The Major Altered Metabolic Pathways in *V. alginolyticus* ATCC17749

Approximately 6.73% (316/4698) of *V. alginolyticus* ATCC17749 genes were expressed differently in the experimental group compared with the control group. Among these, 238 genes showed higher transcription levels (FC $\geq$ 2.0), and 78 genes were down-regulated (FC $\leq$ 0.5). Based on the comparative transcriptomic analyses, 11 significantly changed

metabolic pathways were identified, including valine, leucine and isoleucine degradation; nitrogen, histidine, tryptophan, glyoxylate and dicarboxylate metabolisms; quorum sensing (QS); lysine degradation; fatty acid degradation; amino sugar and nucleotide sugar metabolism; ABC transporters; and mitogen-activated protein kinase (MAPK) signal pathway (Figure 7).

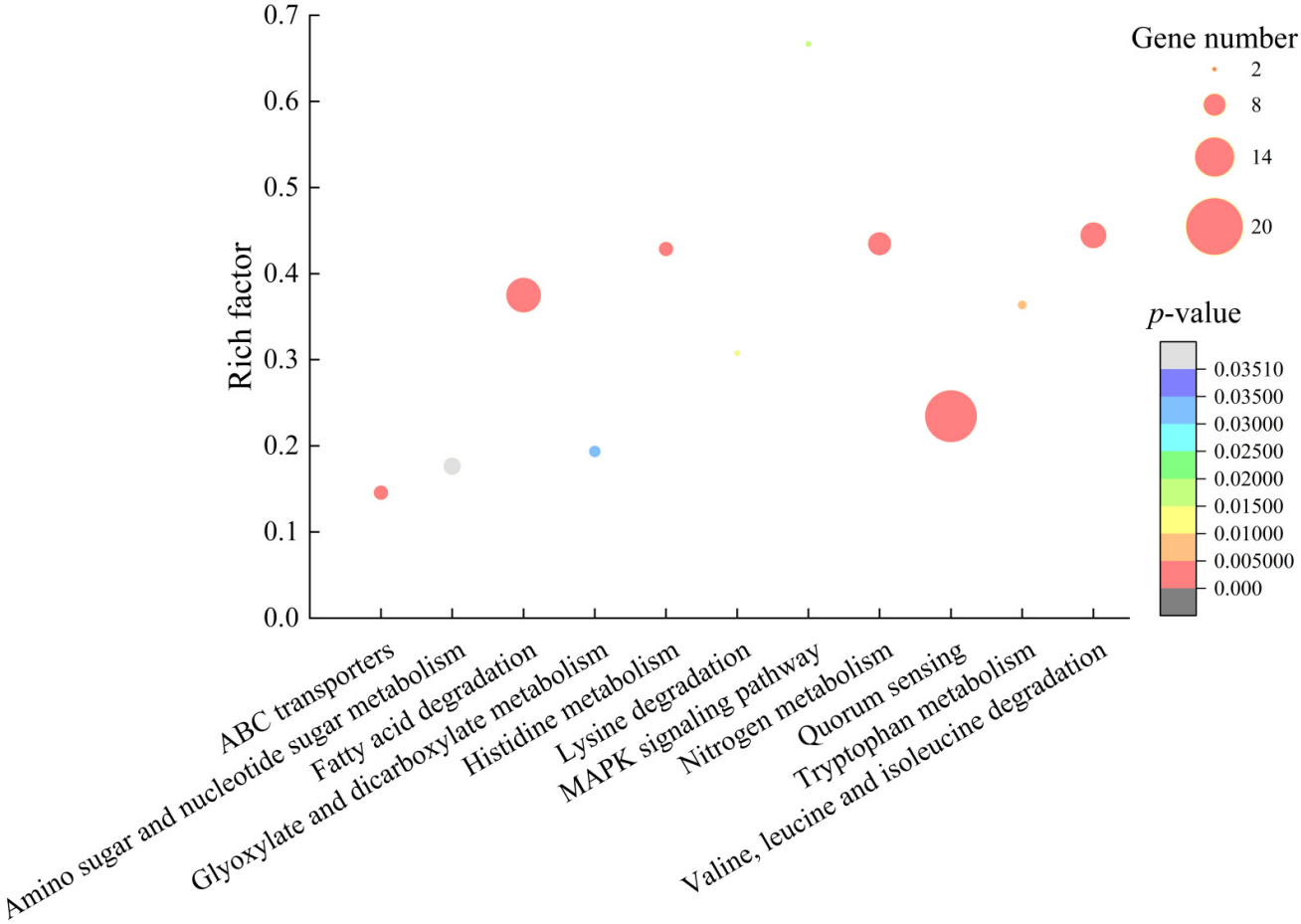


**Figure 7.** The 11 significantly altered metabolic pathways in *V. alginolyticus* ATCC17749 mediated by the CC 1 from *R. madaio* Makino.

Remarkably, approximately 60 DEGs involved in 10 changed metabolic pathways were significantly up-regulated in *V. alginolyticus* ATCC17749 (2.002- to 87.807-fold) ($p < 0.05$) (Table 4). For example, in the valine, leucine and isoleucine degradation, expression of nine DEGs were significantly up-regulated at the transcription level (2.117- to 4.619-fold) ($p < 0.05$); six DEGs encoding key enzymes in the histidine metabolism were also significantly up-regulated (2.001- to 3.187-fold) ($p < 0.05$); similarly, in the tryptophan metabolism, expression of three DEGs were significantly enhanced (2.123- to 5.154-fold) ($p < 0.05$); additionally, in the lysine degradation, expression of a transcriptional regulator (*N646_3623*) and an arginine/lysine/ornithine decarboxylase (*N646_1979*) were significantly up-regulated (2.972- to 3.332-fold) ($p < 0.05$). These four pathways are related to amino acid degradation metabolisms.

Meanwhile, eight DEGs in the nitrogen metabolism were also significantly up-regulated (2.193- to 87.807-fold) ($p < 0.05$), in which, specifically, one DEG encoding a hydroxylamine reductase (*N646_0236*) was greatly enhanced to express (87.807-fold).

ABC transporters are ATP-dependent efflux transporters to transport lipids, metabolites, exogenous substances and other small molecules out of the cell [16]. They are also the main type of transporters associated with bacterial multidrug resistance [17]. In this study, comparative transcriptome analysis revealed 23 DEGs in ABC transporters and QS that were significantly up-regulated in *V. alginolyticus* ATCC17749 (2.104- to 7.585-fold)

($p < 0.05$) (Table 4). ABC transporter can also catalyze the turnover of lipids in the lipid bilayer that play a critical role in the occurrence and functional maintenance of the cell membrane [18]. In this study, the up-regulated expression of these DEGs suggested that the treatment with the CC 1 from *R. madaio* Makino enhanced the bacterial pumping of exogenous and endogenous metabolites to eliminate cell damage.

**Table 4.** Major altered metabolic pathways in *V. alginolyticus* ATCC17749 treated by the CC1 from *R. madaio* Makino.

| Metabolic Pathway | Gene ID | Fold Change | Gene Description |
|---|---|---|---|
| Valine, leucine and isoleucine degradation | *N646_4585* | 2.117 | Acetoacetyl-coenzyme A synthetase |
| | *N646_4506* | 2.127 | Putative 3-hydroxyisobutyrate dehydrogenase |
| | *N646_4019* | 2.293 | Acetoacetyl-coenzyme A synthetase |
| | *N646_4049* | 2.793 | Putative acyl-CoA carboxyltransferase beta chain |
| | *N646_4047* | 3.123 | Putative acyl-CoA carboxylase alpha chain |
| | *N646_4057* | 3.302 | 3-hydroxyisobutyrate dehydrogenase |
| | *N646_4048* | 4.128 | Putative enoyl-CoA hydratase/isomerase |
| | *N646_4053* | 4.602 | Putative aldehyde dehydrogenase |
| | *N646_4050* | 4.619 | Putative acyl-CoA dehydrogenase |
| Nitrogen metabolism | *N646_3727* | 2.193 | Putative oxidoreductase protein |
| | *N646_4426* | 2.656 | Hypothetical protein |
| | *N646_3915* | 5.506 | Periplasmic nitrate reductase |
| | *N646_4365* | 5.657 | Hypothetical protein |
| | *N646_3914* | 6.137 | Periplasmic nitrate reductase%2C cytochrome c-type protein |
| | *N646_4364* | 11.868 | Nitrite reductase [NAD(P)H]%2C small subunit |
| | *N646_1010* | 29.988 | Nitrite reductase periplasmic cytochrome c552 |
| | *N646_0236* | 87.807 | Hydroxylamine reductase |
| Quorum sensing | *N646_0372* | 2.104 | ABC-type spermidine/putrescine transport system%2C permease component II |
| | *N646_2230* | 2.108 | Peptide ABC transporter%2C permease protein |
| | *N646_4026* | 2.258 | Putative ABC transporter%2C membrane spanning protein |
| | *N646_1576* | 2.315 | Peptide ABC transporter%2C periplasmic peptide-binding protein |
| | *N646_0379* | 2.493 | Oligopeptide ABC transporter%2C permease protein |
| | *N646_2228* | 2.531 | Peptide ABC transporter%2C periplasmic peptide-binding protein |
| | *N646_4027* | 2.666 | Putative high-affinity branched-chain amino acid transport permease protein |
| | *N646_0377* | 2.688 | Oligopeptide ABC transporter%2C ATP-binding protein |
| | *N646_1580* | 2.821 | Peptide ABC transporter%2C ATP-binding protein |
| | *N646_0378* | 2.836 | Oligopeptide ABC transporter%2C ATP-binding protein |
| | *N646_4024* | 2.850 | Putative high-affinity branched-chain amino acid transport ATP-binding protein |
| | *N646_0380* | 2.854 | Oligopeptide ABC transporter%2C permease protein |
| | *N646_4025* | 2.951 | Putative long-chain-fatty-acid-CoA ligase |
| | *N646_0381* | 3.075 | Oligopeptide ABC transporter%2C periplasmic oligopeptide-binding protein |
| | *N646_0370* | 3.909 | Putative ATP-binding component of ABC transporter |
| | *N646_4029* | 4.034 | Putative high-affinity branched-chain amino acid transport ATP-binding protein |
| | *N646_0371* | 4.049 | Putative permease of ABC transporter |
| | *N646_0367* | 4.112 | Putative binding protein component of ABC transporter |
| Histidine metabolism | *N646_0312* | 2.001 | Formimidoylglutamase |
| | *N646_0189* | 2.072 | Imidazoleglycerol-phosphate dehydratase/histidinol-phosphatase |
| | *N646_0190* | 2.090 | Imidazole glycerol phosphate synthase subunit HisH |
| | *N646_0313* | 3.141 | Imidazolonepropionase |
| | *N646_0311* | 3.168 | Urocanate hydratase |
| | *N646_0310* | 3.187 | Histidine ammonia-lyase |
| Fatty acid degradation | *N646_1753* | 0.344 | Hypothetical protein |
| | *N646_0066* | 2.033 | Amino acid ABC transporter%2C permease protein |
| | *N646_3145* | 2.064 | Rubredoxin/rubredoxin reductase |
| | *N646_2209* | 2.122 | Acetyl-CoA C-acyltransferase FadA |
| | *N646_3116* | 2.163 | Maltose ABC transporter periplasmic protein |
| | *N646_3117* | 2.319 | Maltose/maltodextrin ABC transporter%2C ATP-binding protein |
| | *N646_3389* | 2.793 | Putative ferrichrome ABC transporter (permease) |
| | *N646_1395* | 2.879 | Acyl-CoA dehydrogenase |
| | *N646_4429* | 3.400 | Nitrate ABC transporter nitrate-binding protein |
| | *N646_4028* | 5.585 | Hypothetical protein |
| | *N646_4427* | 6.398 | Hypothetical protein |
| | *N646_3568* | 14.448 | Putative ABC transporter%2C ATP-binding protein |

**Table 4.** *Cont.*

| Metabolic Pathway | Gene ID | Fold Change | Gene Description |
|---|---|---|---|
| ABC transporters | *N646_4485* | 2.173 | Arginine ABC transporter%2C permease protein |
| | *N646_4527* | 3.899 | Putative inner-membrane permease |
| | *N646_4487* | 4.958 | Arginine ABC transporter%2C periplasmic arginine-binding protein |
| | *N646_4488* | 5.676 | Arginine ABC transporter%2C ATP-binding protein |
| | *N646_4486* | 7.585 | ABC-type arginine transport system%2C permease component |
| Tryptophan metabolism | *N646_2210* | 2.123 | Fatty oxidation complex%2C alpha subunit |
| | *N646_3629* | 2.155 | Tryptophanase |
| | *N646_4052* | 5.154 | Putative acyl-CoA thiolase |
| Lysine degradation | *N646_3623* | 2.972 | Transcriptional regulator |
| | *N646_1979* | 3.332 | Arginine/lysine/ornithine decarboxylase |
| MAPK signaling pathway | *N646_2909* | 0.123 | Cation transport ATPase%2C E1-E2 family protein |
| | *N646_3134* | 0.369 | Catalase |
| Glyoxylate and dicarboxylate metabolism | *N646_1965* | 2.122 | Acetyl-coenzyme A synthetase |
| | *N646_2741* | 2.135 | Isocitrate lyase |
| | *N646_2740* | 2.88 | Malate synthase |
| | *N646_3637* | 3.006 | Malate synthase |
| Amino sugar and nucleotide sugar metabolism | *N646_4226* | 0.400 | Glucose-1-phosphate adenylyltransferase |
| | *N646_1583* | 2.322 | Beta-*N*-hexosaminidase |
| | *N646_3834* | 2.610 | Hypothetical protein |
| | *N646_1582* | 3.440 | Ptative *N*-acetylglucosamine kinase |
| | *N646_4346* | 4.386 | Ptative mannose-6-phosphate isomerase |
| | *N646_3455* | 5.366 | Hpothetical protein |

In contrast, all DEGs in the MAPK signaling pathway were significantly inhibited (0.123- to 0.369-fold) ($p < 0.05$) (Table 4), which likely led to a highly toxic reactive oxygen species (ROS) accumulation and cell damage.

### 2.6.2. The Major Altered Metabolic Pathways in *V. parahaemolyticus* ATCC17802

Approximately 19.62% (917/4,674) of *V. parahaemolyticus* ATCC17802 genes were expressed differently in the experimental group compared with the control group. Among these, 128 genes showed higher transcription levels (FC $\geq$ 2.0), and 789 genes were down-regulated (FC $\leq$ 0.5). Comparative transcriptome analyses revealed 20 significantly changed metabolic pathways, including methane, nitrogen, glycerolipid, propanoate, sulfur, starch and sucrose, taurine and hypotaurine, phosphonate and phosphinate, and biotin metabolisms; glucagon, and hypoxia inducible factor-1 (HIF-1) signaling pathway; benzoate and ethylbenzene degradation; glycolysis/gluconeogenesis; flagellar assembly; apoptosis; bacterial chemotaxis; cationic antimicrobial peptide (CAMP) resistance; necroptosis, and RNA transport (Figure 8).

Notably, approximately 77 DEGs involved in 12 changed metabolic pathways were significantly down-regulated (0.05- to 0.491-fold) ($p < 0.05$) (Table 5). For example, in the glycolysis/gluconeogenesis, except for an up-regulated 2-oxo acid dehydrogenase subunit E2 (*VP_RS18295*), the other seven DEGs were significantly down-regulation (0.087- to 0.433-fold) ($p < 0.05$); in the propanoate metabolic pathway, express of four DEGs were significantly depressed (0.051- to 0.240-fold) ($p < 0.05$); in the starch and sucrose metabolisms, except for a 4-alpha-glucono transfer (*VP_RS22910*), the other five DEGs were significantly down-regulated (0.206- to 0.499-fold) ($p < 0.05$). These three metabolic pathways were related to carbohydrate metabolisms. Their overall down-regulation trend indicated inactive carbon source transportation and/or utilization, which likely resulted in insufficient energy supply.

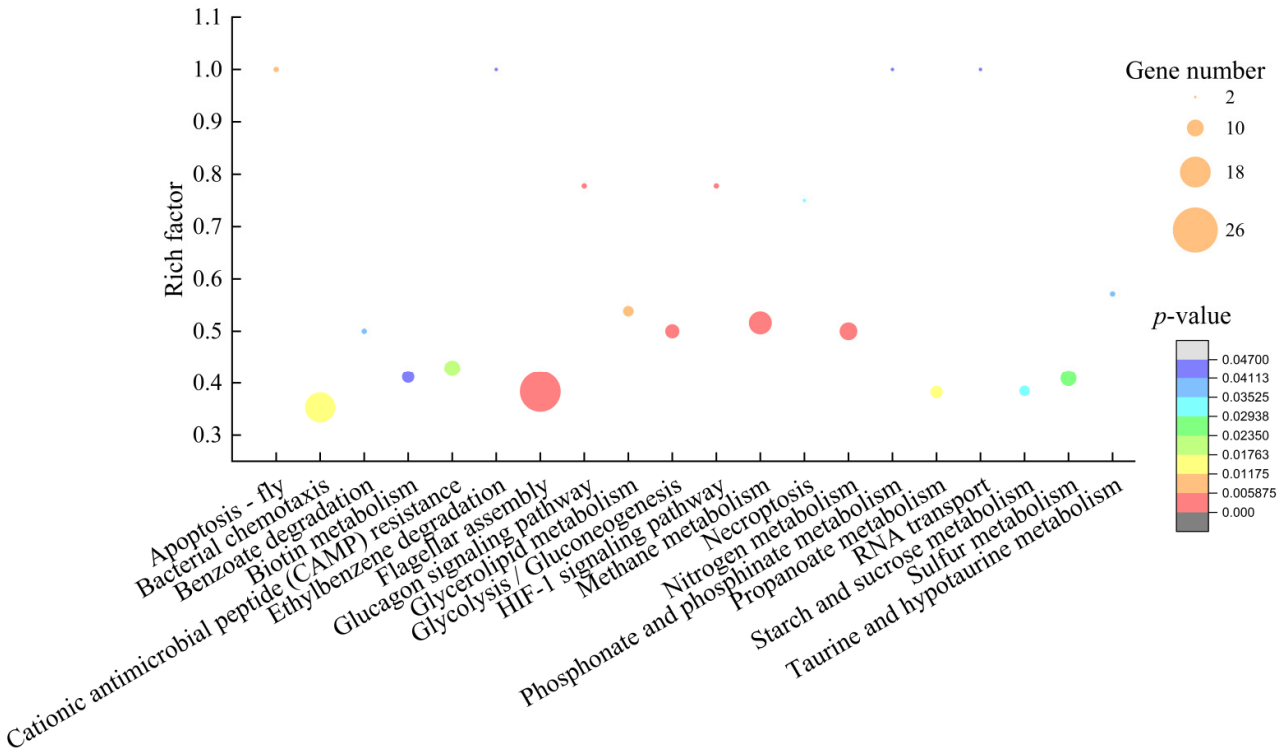


**Figure 8.** The 20 significantly altered metabolic pathways in *V. parahaemolyticus* ATCC17802 mediated by the CC 1 from *R. madaio* Makino.

**Table 5.** Major altered metabolic pathways in *V. parahaemolyticus* ATCC17802 treated by the CC1 from *R. madaio* Makino.

| Metabolic Pathway | Gene ID | Fold Change | Gene Description |
|---|---|---|---|
| Methane metabolism | *VP_RS15865* | 0.091 | NapC/NirT family cytochrome c |
| | *VP_RS15860* | 0.067 | Trimethylamine-*N*-oxide reductase 2 |
| | *VP_RS07325* | 0.224 | Acetate kinase |
| | *VP_RS13930* | 0.206 | 2%2C3-bisphosphoglycerate-independent phosphoglycerate mutase |
| | *VP_RS18135* | 0.104 | Formate dehydrogenase subunit gamma |
| | *VP_RS12615* | 0.320 | Phosphate acetyltransferase |
| | *VP_RS07335* | 0.227 | Trimethylamine-*N*-oxide reductase TorA |
| | *VP_RS15585* | 0.304 | S-(hydroxymethyl)glutathione dehydrogenase/class III alcohol dehydrogenase |
| | *VP_RS05645* | 0.302 | Phosphoglycerate dehydrogenase |
| | *VP_RS07330* | 0.338 | Pentaheme c-type cytochrome TorC |
| | *VP_RS05030* | 0.381 | Molecular chaperone TorD |
| | *VP_RS15580* | 0.412 | S-formylglutathione hydrolase |
| | *VP_RS05640* | 0.342 | 6-phosphofructokinase |
| Glycolysis/Gluconeogenesis | *VP_RS23260* | 0.087 | 6-phospho-beta-glucosidase |
| | *VP_RS12915* | 0.272 | 6-phospho-beta-glucosidase |
| | *VP_RS12215* | 0.310 | Pyruvate dehydrogenase (acetyl-transferring) |
| | *VP_RS12210* | 0.331 | Pyruvate dehydrogenase complex dihydrolipoyllysine-residue acetyltransferase |
| | *VP_RS13410* | 0.406 | Glucose-6-phosphate isomerase |
| | *VP_RS10485* | 0.416 | D-hexose-6-phosphate mutarotase |
| | *VP_RS09910* | 0.433 | Pyruvate kinase |
| | *VP_RS18295* | 2.558 | 2-oxo acid dehydrogenase subunit E2 |
| Flagellar assembly | *VP_RS22540* | 0.055 | Flagellar biosynthesis protein FliQ |
| | *VP_RS16540* | 0.064 | Flagellar basal body rod protein FlgB |
| | *VP_RS16565* | 0.086 | Flagellar basal-body rod protein FlgG |
| | *VP_RS22520* | 0.091 | OmpA family protein |
| | *VP_RS16550* | 0.129 | Flagellar hook assembly protein FlgD |
| | *VP_RS22605* | 0.193 | Flagellar motor stator protein MotA |

**Table 5.** *Cont.*

| Metabolic Pathway | Gene ID | Fold Change | Gene Description |
|---|---|---|---|
| | *VP_RS22545* | 0.210 | Flagellar biosynthetic protein FliR |
| | *VP_RS22575* | 0.225 | Flagellar filament capping protein FliD |
| | *VP_RS22535* | 0.237 | Flagellar type III secretion system pore protein FliP |
| | *VP_RS22490* | 0.265 | Flagellar protein export ATPase FliI |
| | *VP_RS16555* | 0.272 | Flagellar basal body protein FlgE |
| | *VP_RS22590* | 0.281 | Flagellar hook-length control protein FliK |
| | *VP_RS16575* | 0.327 | Flagellar basal body P-ring protein FlgI |
| | *VP_RS10920* | 0.363 | Flagellar M-ring protein FliF |
| | *VP_RS22495* | 0.366 | Flagellar assembly protein H |
| | *VP_RS10900* | 0.386 | Flagella biosynthesis chaperone FliJ |
| | *VP_RS16585* | 0.396 | Flagellar hook-associated protein FlgK |
| | *VP_RS16590* | 0.412 | Flagellar hook-associated protein FlgL |
| | *VP_RS13775* | 0.416 | Sel1 repeat family protein |
| | *VP_RS10835* | 0.429 | RNA polymerase sigma factor FliA |
| | *VP_RS10895* | 0.452 | Flagellar hook-length control protein FliK |
| | *VP_RS03835* | 0.462 | Flagellar hook protein FlgE |
| | *VP_RS03855* | 0.490 | Flagellar basal body P-ring protein FlgI |
| Glucagon signaling pathway | *VP_RS01720* | 0.369 | Pyruvate kinase PykF |
| | *VP_RS18300* | 3.294 | Alpha-ketoacid dehydrogenase subunit beta |
| | *VP_RS22915* | 5.913 | Glycogen/starch/alpha-glucan phosphorylase |
| HIF-1 signaling pathway | *VP_RS10480* | 0.168 | Type I glyceraldehyde-3-phosphate dehydrogenase |
| | *VP_RS14700* | 0.301 | ArsJ-associated glyceraldehyde-3-phosphate dehydrogenase |
| | *VP_RS12650* | 0.479 | Phosphoglycerate kinase |
| Nitrogen metabolism | *VP_RS20240* | 0.126 | Nitrite reductase large subunit NirB |
| | *VP_RS02310* | 0.158 | Glutamate synthase subunit beta |
| | *VP_RS20280* | 0.226 | Nitrate reductase |
| | *VP_RS02315* | 0.236 | Glutamate synthase large subunit |
| | *VP_RS20255* | 0.270 | ABC transporter substrate-binding protein |
| | *VP_RS12190* | 0.418 | Carbonate dehydratase |
| | *VP_RS20915* | 2.061 | Nitrate reductase cytochrome c-type subunit |
| | *VP_RS20910* | 2.197 | Periplasmic nitrate reductase subunit alpha |
| | *VP_RS05780* | 14.974 | Hydroxylamine reductase |
| | *VP_RS09370* | 19.809 | Ammonia-forming nitrite reductase cytochrome c552 subunit |
| Glycerolipid metabolism | *VP_RS01760* | 0.040 | Dihydroxyacetone kinase ADP-binding subunit DhaL |
| | *VP_RS01755* | 0.067 | Dihydroxyacetone kinase subunit DhaK |
| | *VP_RS21295* | 0.193 | Diacylglycerol kinase |
| | *VP_RS11580* | 0.239 | Glycerol kinase GlpK |
| | *VP_RS15810* | 0.431 | Glycerate kinase |
| | *VP_RS05740* | 2.015 | Triacylglycerol lipase |
| Apoptosis | *VP_RS23210* | 0.086 | Alkyl hydroperoxide reductase subunit C |
| | *VP_RS20650* | 0.282 | C-type cytochrome |
| | *VP_RS02795* | 0.415 | Peroxiredoxin C |
| Bacterial chemotaxis | *VP_RS22610* | 0.101 | OmpA family protein |
| | *VP_RS22160* | 0.243 | Methyl-accepting chemotaxis protein |
| | *VP_RS03815* | 0.255 | Protein-glutamate O-methyltransferase |
| | *VP_RS17585* | 0.267 | Methyl-accepting chemotaxis protein |
| | *VP_RS22500* | 0.294 | Flagellar motor switch protein FliG |
| | *VP_RS22100* | 0.337 | Methyl-accepting chemotaxis protein |
| | *VP_RS10915* | 0.356 | Flagellar motor switch protein FliG |
| | *VP_RS05760* | 0.374 | Methyl-accepting chemotaxis protein |
| | *VP_RS10820* | 0.386 | Chemotaxis protein CheA |
| | *VP_RS10825* | 0.389 | Protein phosphatase CheZ |
| | *VP_RS10880* | 0.411 | Flagellar motor switch protein FliN |
| | *VP_RS03810* | 0.415 | Chemotaxis protein CheV |
| | *VP_RS03305* | 0.433 | Flagellar motor protein PomA |
| | *VP_RS10815* | 0.471 | Chemotaxis response regulator protein-glutamate methylesterase |
| | *VP_RS10830* | 0.473 | Chemotaxis response regulator CheY |
| | *VP_RS05310* | 0.486 | Methyl-accepting chemotaxis protein |
| | *VP_RS10800* | 0.491 | Chemotaxis protein CheW |
| Propanoate metabolism | *VP_RS01750* | 0.051 | Glycerol dehydrogenase |
| | *VP_RS04855* | 0.072 | Formate C-acetyltransferase |
| | *VP_RS18985* | 0.119 | Acetyl-CoA carboxylase%2C carboxyltransferase subunit beta |
| | *VP_RS16405* | 0.240 | Aspartate aminotransferase family protein |
| | *VP_RS07930* | 2.084 | 2-methylcitrate synthase |
| | *VP_RS07925* | 2.094 | Fe/S-dependent 2-methylisocitrate dehydratase AcnD |
| | *VP_RS20545* | 2.450 | CoA-acylating methylmalonate-semialdehyde dehydrogenase |

**Table 5.** *Cont.*

| Metabolic Pathway | Gene ID | Fold Change | Gene Description |
|---|---|---|---|
| Cationic antimicrobial peptide (CAMP) resistance | *VP_RS00200* | 0.120 | Multidrug efflux RND transporter permease subunit VmeD |
| | *VP_RS00205* | 0.159 | Multidrug efflux RND transporter periplasmic adaptor subunit VmeC |
| | *VP_RS21260* | 0.344 | Thiol: disuLfide interchange protein DsbA/DsbL |
| | *VP_RS05670* | 0.456 | ATP-binding cassette domain-containing protein |
| | *VP_RS21300* | 0.489 | Phosphoethanolamine-lipid A transferase |
| | *VP_RS05315* | 2.030 | Multidrug efflux RND transporter periplasmic adaptor subunit VmeA |
| | *VP_RS20865* | 2.560 | Multidrug efflux RND transporter periplasmic adaptor subunit VmeY |
| | *VP_RS14065* | 4.124 | Envelope stress sensor histidine kinase CpxA |
| | *VP_RS14060* | 4.705 | Response regulator |
| Sulfur metabolism | *VP_RS07020* | 0.050 | Dimethyl sulfoxide reductase subunit A |
| | *VP_RS07030* | 0.052 | Dimethyl sulfoxide reductase anchor subunit |
| | *VP_RS07025* | 0.058 | Dimethyl sulfoxide reductase subunit B |
| | *VP_RS05930* | 0.110 | Cytochrome subunit of suLfide dehydrogenase |
| | *VP_RS03905* | 0.337 | Cysteine synthase A |
| | *VP_RS13370* | 0.417 | Assimilatory suLfite reductase (NADPH) hemoprotein subunit |
| | *VP_RS13375* | 0.440 | Assimilatory sulfite reductase (NADPH) flavoprotein subunit |
| | *VP_RS01435* | 0.442 | Sulfate adenylyltransferase subunit CysN |
| | *VP_RS01430* | 0.450 | Sulfate adenylyltransferase subunit CysD |
| Starch and sucrose metabolism | *VP_RS12920* | 0.206 | PTS lactose/cellobiose transporter subunit IIA |
| | *VP_RS19165* | 0.393 | Glucose-1-phosphate adenylyltransferase |
| | *VP_RS03410* | 0.474 | Alpha%2Calpha-phosphotrehalase |
| | *VP_RS23025* | 0.498 | Glycogen debranching protein GlgX |
| | *VP_RS03405* | 0.499 | PTS trehalose transporter subunit IIBC |
| | *VP_RS22910* | 4.693 | 4-alpha-glucanotransferase |
| Necroptosis | *VP_RS04005* | 0.261 | Molecular chaperone HtpG |
| | *VP_RS00595* | 0.363 | Glutamate-ammonia ligase |
| Taurine and hypotaurine metabolism | *VP_RS10125* | 0.167 | Acetate kinase |
| | *VP_RS05370* | 0.219 | Alanine dehydrogenase |
| | *VP_RS10130* | 0.244 | Phosphate acetyltransferase |
| Benzoate degradation | *VP_RS20635* | 0.295 | Carboxymuconolactone decarboxylase family protein |
| | *VP_RS20550* | 2.679 | Thiolase family protein |
| | *VP_RS00135* | 2.713 | Fatty acid oxidation complex subunit alpha FadB |
| RNA transport | *VP_RS19430* | 0.440 | Stress response translation initiation inhibitor YciH |
| | *VP_RS01980* | 0.485 | Multifunctional CCA addition/repair protein |
| Phosphonate and phosphinate metabolism | *VP_RS16410* | 0.206 | 2-aminoethylphosphonate–pyruvate Transaminase |
| | *VP_RS16400* | 0.491 | Phosphonoacetaldehyde hydrolase |
| Ethylbenzene degradation | *VP_RS10720* | 2.111 | Acetyl-CoA C-acyltransferase FadI |
| | *VP_RS00130* | 2.465 | Acetyl-CoA C-acyltransferase FadA |
| Biotin metabolism | *VP_RS05435* | 0.057 | Dethiobiotin synthase |
| | *VP_RS21415* | 0.265 | Beta-ketoacyl-ACP reductase |
| | *VP_RS05415* | 0.376 | Adenosylmethionine-8-amino-7-oxononanoate transaminase |
| | *VP_RS05425* | 0.454 | 8-amino-7-oxononanoate synthase |
| | *VP_RS05420* | 0.479 | Biotin synthase BioB |
| | *VP_RS05430* | 0.492 | Malonyl-ACP O-methyltransferase BioC |
| | *VP_RS20520* | 2.061 | SDR family oxidoreductase |

Approximately 44 DEGs involved in six energy metabolism pathways in *V. parahaemolyticus* ATCC17802 were also significantly inhibited ($p < 0.05$). For example, the DEG encoding a pyruvate dehydrogenase complex dihydrolipoyllysine-residue acetyltransferase (*VP_RS12210*) was significantly down-regulated (0.331-fold), which connects glycolysis with tricarboxylic acid cycle (TCA) and plays a key role in glucose metabolism [19]. The down-regulation of this enzyme led to a decrease in ATP production and insufficient energy supply [20], which consequently affected bacterial growth and mobility.

The bacterial flagellum is a complex mobility machine with a diversity of roles in pathogenesis, including attachment, colonization, invasion, maintenance and post-infection dispersal in the host [21,22]. In this study, expression of 23 DEGs involved in three substructures of the flagellum, including the filament, hook and basal body [23], were significantly down-regulated at the transcriptional level in *V. parahaemolyticus* ATCC17802 (0.055- to 0.49-fold) ($p < 0.05$), which indicated the depressed flagellum assembly that led to inactive motility of

*V. parahaemolyticus* ATCC17802. The 17 down-regulated DEGs in the bacterial chemotaxis [24] (0.101- to 0.491-fold) ($p < 0.05$) provided indirect evidence for this result.

Interestingly, 23 DEGs encoding type III secretory system (T3SS) components were also significantly down-regulated (0.055- to 0.490 -fold) ($p < 0.05$). T3SS enables pathogenic bacteria to directly inject effector proteins into host cells, facilitating bacterial colonization in the host [25]. This result suggested that the cytotoxicity of *V. parahaemolyticus* ATCC17802 was significantly reduced after being treated with the CC 1 from *R. madaio* Makino.

Additionally, in the cationic antimicrobial peptide (CAMP) resistance system, five DEGs were significantly inhibited (0.120- to 0.489-fold), including a multidrug efflux RND transporter permease subunit VmeD (*VP_RS00200*), a thiol: disulfide interchange protein DsbA/DsbL (*VP_RS21260*), an ATP-binding cassette domain-containing protein (*VP_RS05670*), a multidrug efflux RND transporter periplasmic adaptor subunit VmeC (*VP_RS00205*), and a phosphoethanolamine-lipid A transferase (*VP_RS21300*) (Table 5). These results indicated poor efficiency of multidrug efflux transport in *V. parahaemolyticus* ATCC17802 after being treated by the CC 1.

In contrast, five DEGs were significantly up-regulated (2.030- to 4.705-fold), e.g., a response regulator (*VP_RS14060*) and an envelope stress sensor histidine kinase CpxA (*VP_RS14065*) (Table 5).

### 2.6.3. The Major Altered Metabolic Pathways in *V. parahaemolyticus* B4-10

Approximately 16.75% (783/4674) of *V. parahaemolyticus* B4-10 genes were expressed differently in the experimental group when compared with the control group. Among these genes, 204 showed higher transcription levels (FC $\geq$ 2.0), and 579 genes were down-regulated (FC $\leq$ 0.5). Based on the comparative transcriptome analysis, five significantly changed metabolic pathways were identified, including styrene degradation, nitrogen metabolism, QS, folate biosynthesis, and histidine metabolism (Figure 9).

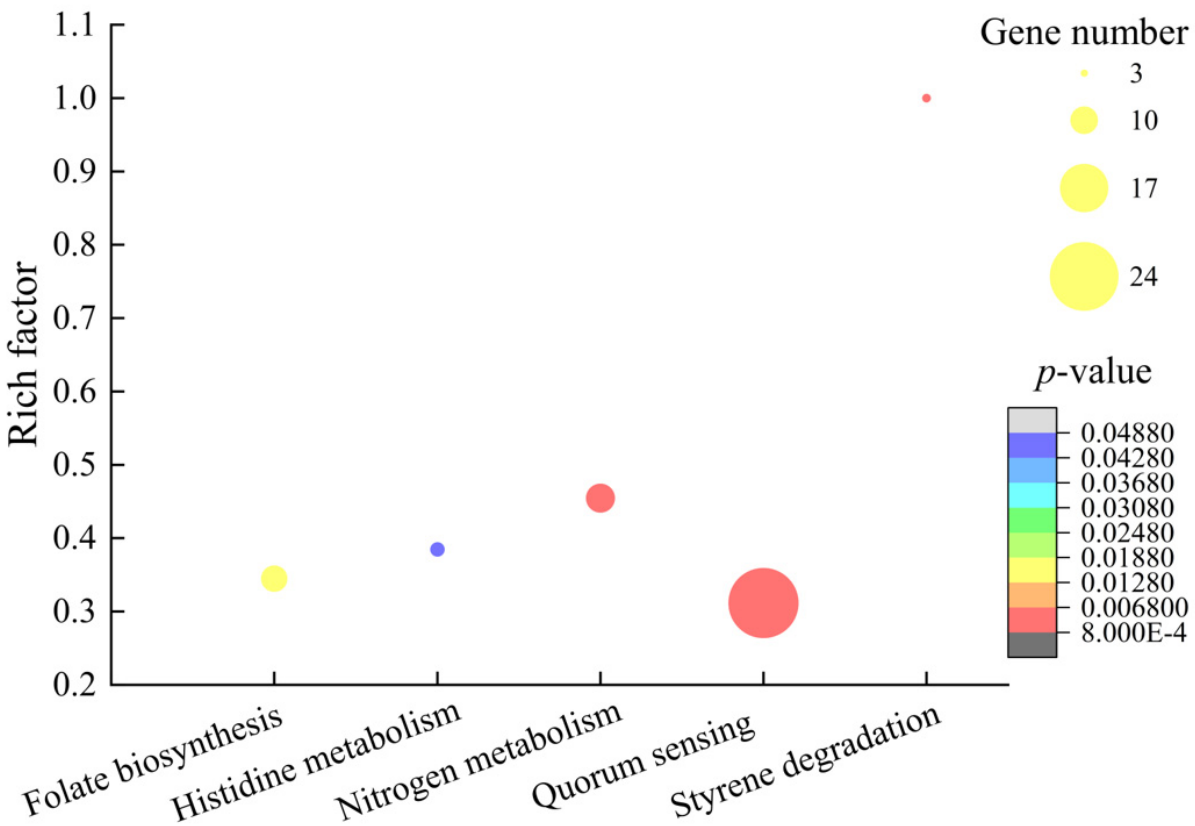


**Figure 9.** The 5 significantly altered metabolic pathways in *V. parahaemolyticus* B4-10 mediated by the CC 1 from *R. madaio* Makino.

Similar to *V. alginolyticus* ATCC17749, the expression of 10 DEGs in the nitrogen metabolism were significantly up-regulated (2.129- to 107.754-fold) ($p < 0.05$) (Table 6). Notably, one DEG encoding a hydroxylamine reductase (*VP_RS05780*) was greatly up-regulated (107.754-fold). This enzyme can reduce hydroxylamine analogs such as methylhydroxylamine and hydroxyquinone as a scavenger of potentially toxic by-products of nitrate metabolism [26]. Moreover, in the histidine metabolism, four DEGs were highly up-regulated (5.106- to 10.231-fold) (Table 6). The enhanced nitrogen metabolism may have supplemented the energy supply in *V. parahaemolyticus* B4-10 after being treated by the CC 1.

**Table 6.** Major altered metabolic pathways in *V. parahaemolyticus* B4-10 treated by the CC1 from *R. madaio* Makino.

| Metabolic Pathway | Gene ID | Fold Change | Gene Description |
|---|---|---|---|
| Styrene degradation | *VP_RS06550* | 0.394 | Homogentisate 1%2C2-dioxygenase |
| | *VP_RS06560* | 0.408 | Maleylacetoacetate isomerase |
| | *VP_RS06555* | 0.471 | Fumarylacetoacetate hydrolase family protein |
| Nitrogen metabolism | *VP_RS20240* | 2.129 | Nitrite reductase large subunit NirB |
| | *VP_RS19890* | 2.518 | Nitrite reductase small subunit NirD |
| | *VP_RS20235* | 2.823 | Nitrite reductase small subunit NirD |
| | *VP_RS20280* | 3.753 | Nitrate reductase |
| | *VP_RS20915* | 3.759 | Nitrate reductase cytochrome c-type subunit |
| | *VP_RS19895* | 3.988 | Nitrite reductase large subunit NirB |
| | *VP_RS20910* | 4.186 | Periplasmic nitrate reductase subunit alpha |
| | *VP_RS20250* | 10.250 | ABC transporter permease |
| | *VP_RS09370* | 29.586 | Ammonia-forming nitrite reductase cytochrome c552 subunit |
| | *VP_RS05780* | 107.754 | Hydroxylamine reductase |
| Quorum sensing | *VP_RS06530* | 0.241 | Oligopeptide ABC transporter permease OppB |
| | *VP_RS06520* | 0.256 | ATP-binding cassette domain-containing protein |
| | *VP_RS06525* | 0.265 | ABC transporter permease subunit |
| | *VP_RS06515* | 0.297 | ATP-binding cassette domain-containing protein |
| | *VP_RS06485* | 0.310 | ABC transporter ATP-binding protein |
| | *VP_RS06495* | 0.346 | ABC transporter permease |
| | *VP_RS06535* | 0.362 | Peptide ABC transporter substrate-binding protein |
| | *VP_RS20670* | 0.368 | ABC transporter ATP-binding protein |
| | *VP_RS06490* | 0.370 | ABC transporter permease |
| | *VP_RS20680* | 0.381 | Branched-chain amino acid ABC transporter permease |
| | *VP_RS06470* | 0.388 | Polyamine ABC transporter substrate-binding protein |
| | *VP_RS21025* | 0.416 | Autoinducer 2-binding periplasmic protein LuxP |
| | *VP_RS20695* | 0.455 | ABC transporter ATP-binding protein |
| | *VP_RS01695* | 0.468 | Long-chain fatty acid–CoA ligase |
| | *VP_RS20675* | 0.475 | ABC transporter substrate-binding protein |
| | *VP_RS00850* | 0.495 | ABC transporter ATP-binding protein |
| | *VP_RS12050* | 2.098 | ABC transporter ATP-binding protein |
| | *VP_RS15305* | 2.117 | GTP cyclohydrolase II |
| | *VP_RS22315* | 2.159 | ABC transporter ATP-binding protein |
| | *VP_RS12040* | 2.232 | ABC transporter permease |
| | *VP_RS08360* | 2.551 | Two-component sensor histidine kinase |
| | *VP_RS22015* | 2.976 | Response regulator transcription factor |
| | *VP_RS08355* | 3.014 | Response regulator |
| | *VP_RS16930* | 3.141 | Permease |
| Folate biosynthesis | *VP_RS17975* | 0.476 | Phenylalanine 4-monooxygenase |
| | *VP_RS09130* | 0.494 | Aminodeoxychorismate synthase component I |
| | *VP_RS03365* | 0.491 | NADPH-dependent 7-cyano-7-deazaguanine reductase QueF |
| | *VP_RS07885* | 0.497 | 7-cyano-7-deazaguanine synthase QueC |
| | *VP_RS09170* | 0.389 | 6-carboxytetrahydropterin synthase QueD |
| | *VP_RS13730* | 0.433 | Aminodeoxychorismate/anthranilate synthase component II |
| | *VP_RS07890* | 0.484 | 7-carboxy-7-deazaguanine synthase QueE |
| | *VP_RS17980* | 0.432 | 4a-hydroxytetrahydrobiopterin dehydratase |

**Table 6.** *Cont.*

| Metabolic Pathway | Gene ID | Fold Change | Gene Description |
|---|---|---|---|
| | *VP_RS01970* | 0.431 | 2-amino-4-hydroxy-6-hydroxymethyldihydropteridine diphosphokinase |
| Histidine metabolism | *VP_RS06185* | 10.231 | Urocanate hydratase |
| | *VP_RS06180* | 6.284 | Histidine ammonia-lyase |
| | *VP_RS06195* | 6.998 | Imidazolonepropionase |
| | *VP_RS06190* | 5.106 | Formimidoylglutamase |
| | *VP_RS05565* | 0.496 | Bifunctional phosphoribosyl-AMP cyclohydrolase/phosphoribosyl-ATP diphosphatase HisIE |

2.6.4. The Major Altered Metabolic Pathways in *B. cereus* A1-1

Approximately 12.57% (720/5730) of *B. cereus* A1-1 genes were expressed differently in the experimental group. Among these genes, 178 showed higher transcription levels (FC $\geq$ 2.0), and 542 genes were down-regulated (FC $\leq$ 0.5). The comparative transcriptome analysis revealed 17 significantly changed metabolic pathways, including flagellar assembly; bacterial chemotaxis; two-component system (TCS); thiamine and nitrogen metabolisms; ABC transporters; arginine biosynthesis; fatty acid degradation; alanine, aspartate and glutamate metabolism; riboflavin metabolism; HIF-1 signaling pathway; glycolysis/gluconeogenesis; butanoate, pyrimidine, and propanoate metabolisms; benzoate degradation; and inositol phosphate metabolism (Figure 10).

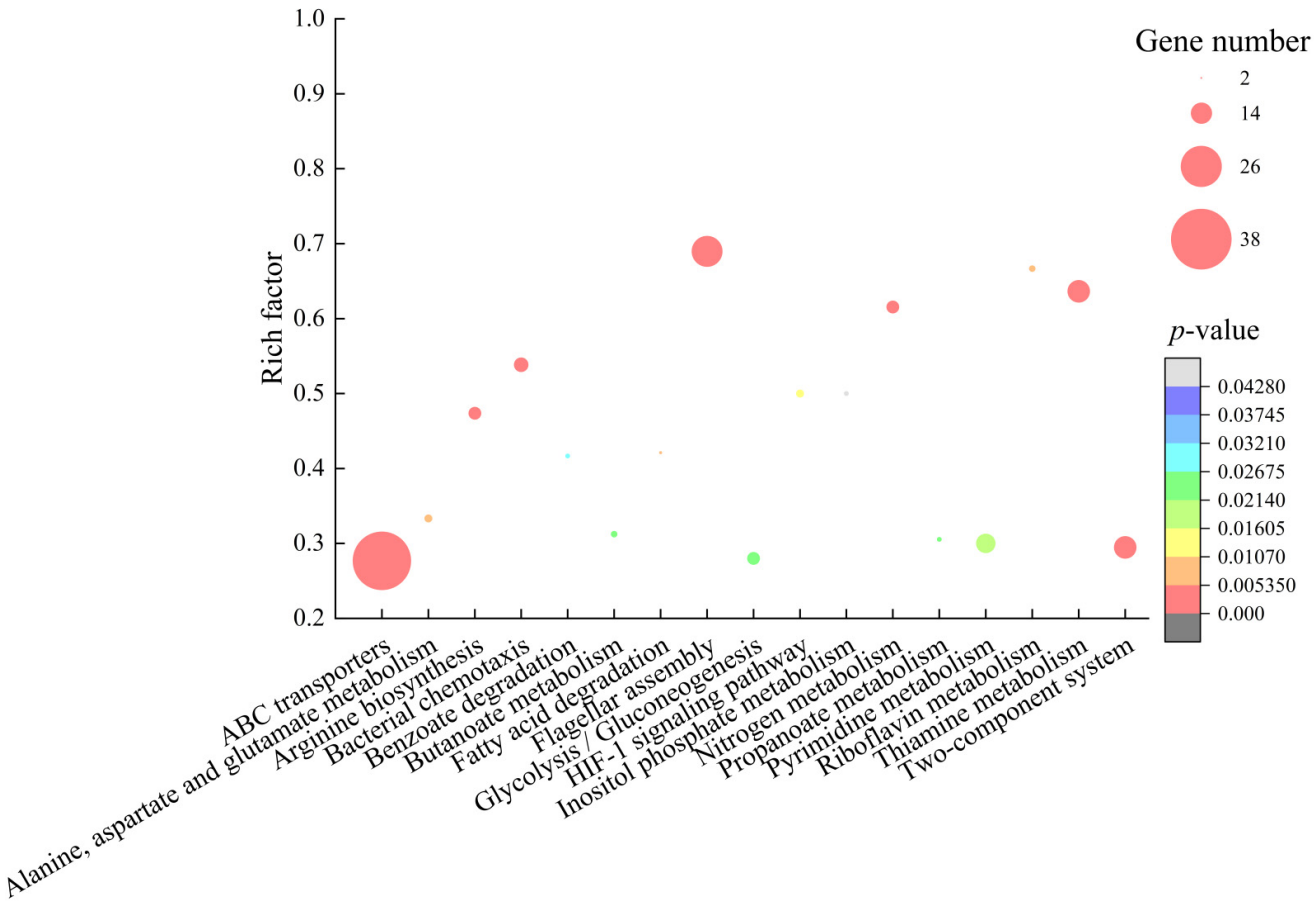


**Figure 10.** The 17 significantly altered metabolic pathways in *B. cereus* A1-1 mediated by the CC 1 from *R. madaio* Makino.

Similar to the other bacterial strains tested, expression of 12 DEGs involved in the nitrogen metabolism and riboflavin metabolism were significantly up-regulated in *B. cereus*

A1-1 (3.325- to 150.780-fold) ($p < 0.05$) (Table 7). Specifically, the DEG encoding a hydroxylamine reductase (*BCN_RS16540*) was also greatly enhanced to express in *B. cereus* A1-1 (150.780-fold).

**Table 7.** Major altered metabolic pathways in *B. cereus* A1-1 treated by the CC1 from *R. madaio* Makino.

| Metabolic Pathway | Gene ID | Fold Change | Gene Description |
|---|---|---|---|
| Flagellar assembly | *BCN_RS08555* | 0.038 | Flagellar assembly protein FliH |
| | *BCN_RS08605* | 0.045 | Flagellin |
| | *BCN_RS08610* | 0.072 | Flagellin |
| | *BCN_RS08640* | 0.108 | Flagellar type III secretion system pore protein FliP |
| | *BCN_RS08550* | 0.113 | Flagellar motor switch protein FliG |
| | *BCN_RS22265* | 0.115 | Flagellar motor stator protein MotA |
| | *BCN_RS22260* | 0.143 | Flagellar motor protein MotB |
| | *BCN_RS08545* | 0.154 | Flagellar M-ring protein FliF |
| | *BCN_RS08470* | 0.158 | Flagellar motor switch protein |
| | *BCN_RS08560* | 0.158 | Flagellar protein export ATPase FliI |
| | *BCN_RS08535* | 0.173 | Flagellar basal body rod protein FlgC |
| | *BCN_RS08670* | 0.188 | Flagellar basal-body rod protein FlgG |
| | *BCN_RS08520* | 0.196 | Flagellar protein FliS |
| | *BCN_RS08530* | 0.197 | Flagellar basal body rod protein FlgB |
| | *BCN_RS08625* | 0.200 | Flagellar motor switch protein FliM |
| | *BCN_RS08660* | 0.230 | Flagellar biosynthesis protein FlhA |
| | *BCN_RS08510* | 0.241 | Flagellar hook-associated protein 3 |
| | *BCN_RS08655* | 0.392 | Flagellar type III secretion system protein FlhB |
| | *BCN_RS08650* | 0.438 | Flagellar type III secretion system protein FliR |
| Bacterial chemotaxis | *BCN_RS10010* | 0.063 | Methyl-accepting chemotaxis protein |
| | *BCN_RS03675* | 0.088 | Methyl-accepting chemotaxis protein |
| | *BCN_RS02280* | 0.185 | Methyl-accepting chemotaxis protein |
| | *BCN_RS08460* | 0.186 | Response regulator |
| | *BCN_RS08625* | 0.200 | Flagellar motor switch protein FliM |
| | *BCN_RS25160* | 0.265 | DUF4077 domain-containing protein |
| | *BCN_RS24975* | 0.321 | Methyl-accepting chemotaxis protein |
| | *BCN_RS08595* | 0.357 | Chemotaxis protein |
| | *BCN_RS08455* | 0.474 | OmpA family protein |
| Two-component system | *BCN_RS27005* | 0.136 | Respiratory nitrate reductase subunit gamma |
| | *BCN_RS26190* | 0.152 | Cytochrome d ubiquinol oxidase subunit II |
| | *BCN_RS23710* | 0.219 | Potassium-transporting ATPase subunit KdpA |
| | *BCN_RS27000* | 0.231 | Acetyl-CoA C-acyltransferase |
| | *BCN_RS23715* | 0.258 | Methyl-accepting chemotaxis protein |
| | *BCN_RS04080* | 0.385 | Nitrate reductase molybdenum cofactor assembly chaperone |
| | *BCN_RS15080* | 0.401 | Response regulator |
| | *BCN_RS04090* | 0.419 | Methyl-accepting chemotaxis protein |
| | *BCN_RS07505* | 2.006 | Phosphate ABC transporter substrate-binding protein PstS |
| | *BCN_RS26540* | 2.297 | Cytochrome ubiquinol oxidase subunit I |
| | *BCN_RS17290* | 2.348 | Chemotaxis protein CheA |
| | *BCN_RS02700* | 3.703 | Antiholin-like murein hydrolase modulator LrgA |
| | *BCN_RS10795* | 4.600 | Acetyl-CoA C-acetyltransferase |
| | *BCN_RS07495* | 5.804 | Hypothetical protein |
| Thiamine metabolism | *BCN_RS29465* | 0.031 | TenA family transcriptional regulator |
| | *BCN_RS02365* | 0.205 | Thiamine phosphate synthase |
| | *BCN_RS04005* | 0.224 | Thiaminase II |
| | *BCN_RS04040* | 0.274 | Thiazole synthase |
| | *BCN_RS04030* | 0.282 | Glycine oxidase ThiO |
| | *BCN_RS04050* | 0.304 | Bifunctional hydroxymethylpyrimidine kinase/phosphomethylpyrimidine kinase |
| | *BCN_RS04025* | 0.310 | Thiazole tautomerase TenI |
| | *BCN_RS25935* | 0.320 | Phosphomethylpyrimidine synthase ThiC |
| | *BCN_RS21485* | 0.342 | Alkaline phosphatase |
| | *BCN_RS12695* | 0.397 | Thiaminase II |

**Table 7.** *Cont.*

| Metabolic Pathway | Gene ID | Fold Change | Gene Description |
|---|---|---|---|
| | *BCN_RS02360* | 0.407 | Hydroxyethylthiazole kinase |
| | *BCN_RS10005* | 0.407 | Ribosome small subunit-dependent GTPase A |
| | *BCN_RS22955* | 0.433 | Cysteine desulfurase |
| | *BCN_RS02660* | 0.457 | Acetylornithine deacetylase |
| ABC transporters | *BCN_RS03130* | 0.051 | Amino acid ABC transporter permease |
| | *BCN_RS14125* | 0.051 | Glycine betaine ABC transporter substrate-binding protein |
| | *BCN_RS15895* | 0.056 | Substrate-binding domain-containing protein |
| | *BCN_RS06920* | 0.179 | ABC transporter ATP-binding protein |
| | *BCN_RS17880* | 0.205 | Ribose ABC transporter ATP-binding protein RbsA |
| | *BCN_RS01110* | 0.221 | Amino acid ABC transporter ATP-binding protein |
| | *BCN_RS06915* | 0.225 | Peptide ABC transporter substrate-binding protein |
| | *BCN_RS01100* | 0.258 | Amino acid ABC transporter ATP-binding protein |
| | *BCN_RS04010* | 0.263 | Phosphate ABC transporter permease PstA |
| | *BCN_RS08770* | 0.268 | Peptide ABC transporter substrate-binding protein |
| | *BCN_RS14120* | 0.268 | BMP family protein |
| | *BCN_RS20515* | 0.272 | ABC transporter ATP-binding protein |
| | *BCN_RS03855* | 0.278 | Phosphonate ABC transporter ATP-binding protein |
| | *BCN_RS01165* | 0.282 | Molybdate ABC transporter permease subunit |
| | *BCN_RS20525* | 0.283 | ABC transporter ATP-binding protein |
| | *BCN_RS21100* | 0.320 | Metal ABC transporter substrate-binding protein |
| | *BCN_RS04020* | 0.322 | ABC transporter substrate-binding protein |
| | *BCN_RS04015* | 0.326 | Phosphate ABC transporter permease subunit PstC |
| | *BCN_RS03845* | 0.330 | ATP-binding cassette domain-containing protein |
| | *BCN_RS03850* | 0.347 | Phosphate ABC transporter ATP-binding protein |
| | *BCN_RS24655* | 0.347 | Transporter substrate-binding domain-containing protein |
| | *BCN_RS01125* | 0.351 | Putative 2-aminoethylphosphonate ABC transporter ATP-binding protein |
| | *BCN_RS20520* | 0.355 | Aliphatic sulfonate ABC transporter substrate-binding protein |
| | *BCN_RS18335* | 0.379 | Iron ABC transporter permease |
| | *BCN_RS09350* | 0.405 | Energy-coupling factor transporter transmembrane protein EcfT |
| | *BCN_RS24665* | 0.405 | Putative 2-aminoethylphosphonate ABC transporter substrate-binding protein |
| | *BCN_RS01160* | 0.413 | Molybdate ABC transporter substrate-binding protein |
| | *BCN_RS04750* | 0.458 | ABC transporter permease |
| | *BCN_RS01870* | 0.465 | ABC transporter permease |
| | *BCN_RS17755* | 0.470 | Methionine ABC transporter substrate-binding lipoprotein MetQ |
| | *BCN_RS03600* | 0.487 | Phosphate ABC transporter substrate-binding protein PstS |
| | *BCN_RS09570* | 0.487 | Peptide ABC transporter substrate-binding protein |
| | *BCN_RS10085* | 0.487 | Sugar ABC transporter permease |
| | *BCN_RS09640* | 4.508 | Thiol reductant ABC exporter subunit CydC |
| | *BCN_RS26090* | 14.65 | ABC transporter substrate-binding protein |
| | *BCN_RS13495* | 20.285 | MetQ/NlpA family ABC transporter substrate-binding protein |
| Arginine biosynthesis | *BCN_RS20420* | 0.070 | N-acetyl-gamma-glutamyl-phosphate reductase |
| | *BCN_RS20400* | 0.117 | Ornithine carbamoyltransferase |
| | *BCN_RS20410* | 0.159 | Acetylglutamate kinase |
| | *BCN_RS20405* | 0.171 | Acetylornithine transaminase |
| | *BCN_RS20415* | 0.271 | Bifunctional glutamate N-acetyltransferase/amino-acid acetyltransferase ArgJ |
| | *BCN_RS00945* | 0.281 | Arginase |
| | *BCN_RS22860* | 0.292 | Argininosuccinate lyase |
| | *BCN_RS22865* | 0.486 | Argininosuccinate synthase |
| Nitrogen metabolism | *BCN_RS07150* | 0.365 | Nitronate monooxygenase |
| | *BCN_RS10835* | 5.001 | Nitrate transporter NarK |
| | *BCN_RS10790* | 6.281 | Nitrate reductase subunit beta |
| | *BCN_RS10800* | 7.880 | Respiratory nitrate reductase subunit gamma |
| | *BCN_RS10785* | 8.675 | Nitrate reductase subunit alpha |
| | *BCN_RS10870* | 8.912 | Nitrite reductase small subunit NirD |

**Table 7.** *Cont.*

| Metabolic Pathway | Gene ID | Fold Change | Gene Description |
|---|---|---|---|
| | *BCN_RS10875* | 15.156 | NADPH-nitrite reductase large subunit |
| | *BCN_RS16540* | 150.780 | Hydroxylamine reductase |
| Riboflavin metabolism | *BCN_RS20310* | 3.325 | Bifunctional diaminohydroxyphosphoribosylaminopyrimidine deaminase/5-Amino-6-(5-phosphoribosylamino) uracil reductase RibD |
| | *BCN_RS20320* | 4.247 | Bifunctional 3%2C4-dihydroxy-2-butanone 4-phosphate synthase/GTP Cyclohydrolase II |
| | *BCN_RS20325* | 4.361 | 6%2C7-dimethyl-8-ribityllumazine synthase |
| | *BCN_RS20315* | 4.769 | Riboflavin synthase subunit alpha |
| Pyrimidine metabolism | *BCN_RS15125* | 0.304 | 5′-nucleotidase C-terminal domain-containing protein |
| | *BCN_RS24625* | 0.355 | Bifunctional metallophosphatase/5′-nucleotidase |
| | *BCN_RS18815* | 0.381 | Carbamoyl-phosphate synthase large subunit |
| | *BCN_RS18820* | 0.406 | Carbamoyl phosphate synthase small subunit |
| | *BCN_RS18795* | 0.419 | Orotate phosphoribosyltransferase |
| | *BCN_RS18805* | 0.430 | Dihydroorotate oxidase B catalytic subunit |
| | *BCN_RS18800* | 0.438 | Orotidine-5′-phosphate decarboxylase |
| | *BCN_RS18810* | 0.441 | Dihydroorotate oxidase B electron transfer subunit |
| | *BCN_RS20265* | 0.445 | 5′-nucleotidase C-terminal domain-containing protein |
| | *BCN_RS18825* | 0.449 | Dihydroorotase |
| | *BCN_RS07895* | 0.462 | Nucleoside-diphosphate kinase |
| | *BCN_RS09440* | 0.473 | Pyrimidine-nucleoside phosphorylase |
| HIF-1 signaling pathway | *BCN_RS24725* | 0.191 | L-lactate dehydrogenase |
| | *BCN_RS25405* | 2.598 | Phosphoglycerate kinase |
| | *BCN_RS25410* | 2.736 | Type I glyceraldehyde-3-phosphate dehydrogenase |
| | *BCN_RS25390* | 3.143 | phosphopyruvate hydratase |
| | *BCN_RS24095* | 5.531 | L-lactate dehydrogenase |
| Fatty acid degradation | *BCN_RS17445* | 0.340 | Acetyl-CoA C-acetyltransferase |
| | *BCN_RS17450* | 0.456 | Acyl-CoA synthetase |
| Alanine, aspartate and glutamate metabolism | *BCN_RS08845* | 0.353 | Glutaminase A |
| | *BCN_RS08855* | 0.361 | Hypothetical protein |
| | *BCN_RS19905* | 0.420 | Carbon-nitrogen family hydrolase |
| | *BCN_RS15030* | 0.486 | Asparaginase |
| | *BCN_RS03305* | 0.498 | Aspartate ammonia-lyase |
| | *BCN_RS00970* | 2.986 | Glutamine–fructose-6-phosphate transaminase (isomerizing) |
| | *BCN_RS03230* | 7.200 | Alanine dehydrogenase |
| Benzoate degradation | *BCN_RS26535* | 2.191 | 3-hydroxybutyryl-CoA dehydrogenase |
| | *BCN_RS24780* | 2.199 | Acetyl-CoA C-acetyltransferase |
| | *BCN_RS24785* | 2.285 | 3-hydroxyacyl-CoA dehydrogenase/enoyl-CoA hydratase family protein |
| Glycolysis/Gluconeogenesis | *BCN_RS08815* | 0.225 | Histidine phosphatase family protein |
| | *BCN_RS21600* | 0.299 | Bifunctional acetaldehyde-CoA/alcohol dehydrogenase |
| | *BCN_RS11285* | 0.411 | Alcohol dehydrogenase AdhP |
| | *BCN_RS28275* | 0.413 | S-(hydroxymethyl)glutathione dehydrogenase/class III alcohol dehydrogenase |
| | *BCN_RS22940* | 0.489 | Acyl-CoA ligase |
| | *BCN_RS26420* | 2.666 | PTS glucose transporter subunit IIA |
| | *BCN_RS25395* | 2.901 | 2%2C3-bisphosphoglycerate-independent phosphoglycerate mutase |
| | *BCN_RS25815* | 5.561 | 6-phospho-beta-glucosidase |
| Inositol phosphate metabolism | *BCN_RS18155* | 0.186 | Phosphatidylinositol diacylglycerol-lyase |
| | *BCN_RS03640* | 0.245 | Phospholipase C |
| | *BCN_RS25400* | 2.616 | Triose-phosphate isomerase |
| Butanoate metabolism | *BCN_RS02750* | 0.158 | Formate C-acetyltransferase |
| | *BCN_RS07305* | 0.199 | Acetolactate synthase large subunit |
| | *BCN_RS11410* | 0.359 | Acetate CoA-transferase subunit alpha |

**Table 7.** *Cont.*

| Metabolic Pathway | Gene ID | Fold Change | Gene Description |
|---|---|---|---|
| Propanoate metabolism | *BCN_RS11415* | 0.382 | CoA transferase subunit B |
| | *BCN_RS04800* | 2.474 | Alpha-acetolactate decarboxylase |
| | *BCN_RS18555* | 0.407 | ADP-forming succinate–CoA ligase subunit beta |
| | *BCN_RS07995* | 0.451 | Methylglyoxal synthase |
| | *BCN_RS18550* | 0.467 | Succinate-CoA ligase subunit alpha |

Conversely, 69 DEGs involved in the flagellar assembly, bacterial chemotaxis, ABC transporters, and TCS were significantly down-regulated at the transcription level in *B. cereus* A1-1 (0.038- to 0.487-fold) ($p < 0.05$) (Table 7), similar to the other bacterial strains treated with the CC1. For example, in the flagellar assembly, expression of 19 DEGs were significantly depressed (0.038- to 0.438-fold) ($p < 0.05$); 9 DEGs in bacterial chemotaxis were significantly down-regulated (0.063- to 0.474-fold); and expression of 33 DEGs in ABC transporters were significantly inhibited (0.051- to 0.487-fold).

Approximately eight DEGs in the TCSs were significantly down-regulated. TCSs are widespread regulatory systems that can help bacteria to control their cellular functions and respond to a diverse range of stimuli [27]. In this study, in the HIF-1 signaling pathway, the expression of a L-lactate dehydrogenase (*BCN_RS24725*) was also significantly down-regulated (0.191-fold). These results indicated the inhibited signal transduction systems in *B. cereus* A1-1.

Additionally, 17 DEGs in the arginine biosynthesis, thiamine metabolism, and alanine, aspartate and glutamate metabolism were all significantly down-regulated (0.031- to 0.498-fold) ($p < 0.05$) (Table 7), which suggested the inhibited energy metabolism in *B. cereus* A1-1 after being treated by the CC 1 from *R. madaio* Makino.

## 3. Materials and Methods

### *3.1. Bacterial Strains and Culture Conditions*

Bacterial strains and culture media used in this study are listed in Table S1. Bacterial culture media were purchased as described previously [28]. *Vibrio* strains were inoculated in media (pH 8.4–8.5) with 3.0% NaCl, while non-*Vibrios* in media (pH 7.0–7.2) with 1% NaCl [28].

### *3.2. Extraction of Bioactive Substances from R. madaio Makino*

*R. madaio* Makino was collected in Lishui City (27°25′37′′ N, 118°41′28′′ E), Zhejiang Province, China in September of 2020. A 500 g of fresh leaf and stem tissues of *R. madaio* Makino was washed clean, dried at room temperature, and then freeze-dried using ALPHA 2-4 LD Plus Freeze Dryer (Martin Christ, Osterode, Germany) at −80 °C for 48 h. The freeze-dried material was crushed using FW-135 High-Speed Crusher (Beijing Kangtuo Medical Instruments Co., Ltd., Beijing, China) and passed through 300 mesh screen. Then, 10.0 g of the powder was mixed with 99-mL chloroform: methanol (2:1, *v/v*, analytical grade, Merck KGaA, Darmstadt, Germany) at a solid to liquid ratio of 1.10 (*m/v*) for 5 h [29]. A 60 mL of $H_2O$ (Analytical grade, Merck KGaA, Darmstadt,,Germany) was then added, fully mixed, and then sonicated using Scientz IID ULtrasonic Cell Crusher (SCIENT Z, Ningbo, China) at the following parameters: power: 300 W; ultrasonic on time: 1 s; ultrasonic off time: 1 s; working time: 20 min; and probe size: 6 mm. The sonicated mixture was filtered through 20–25 μm membrane (Shanghai Sangon Biological Engineeing Technology and Service Co., Ltd., Shanghai, China), and the filtration was collected for the secondary extraction. The methanol phase was separated from the chloroform phase and then individually evaporated, concentrated on pasting using Rotary Evaporator (IKA, Staufen, Germany).

### *3.3. Antimicrobial Susceptibility Assay*

Susceptibility of bacterial strains (Table S1) to the extracts from *R. madaio* Makino was determined according to the method issued by Clinical and Laboratory Standards

Institute (CLSI) (2018, CLSI, M100-S23) using Mueller-Hinton (M-H) agar (CM337) and Mueller-Hinton broth (M391) (OXOID, Basingstoke, UK). Briefly, a 10 μL of crude extracts (500 μg/mL) was added onto each blank disc (6 mm, OXOID, Basingstoke, UK) on MH ager plates. The gentamicin disc (10 μg, OXOID, Basingstoke, UK) was used as a positive control, while the methanol-phase with water and chloroform-phase with ethanol was a negative control, respectively. The plates were incubated at 37 °C for 12 h. Bacteriostatic activity was evaluated by measuring diameters of bacteriostatic circles.

Broth dilution testing (microdilution) (2018, CLSI, M100-S18) was used to determine MICs of the extracts. Briefly, a 100 μL/well of the extracts (1024 μg/mL) was serially diluted, mixed with 100 μL/well of Mueller-Hinton broth (CM337) and 10 μL/well of bacteria strain ($1.5 \times 10^6$ colony-forming unit (CFU)/mL), and then incubated at 37 °C for 12 h [30]. The MIC was defined as the lowest concentration of a particular antibacterial agent that inhibits bacterial growth (2018, CLSI, M100-S18). The standard solution of gentamicin (100 μg/mL) was purchased from National Standard Material Information Center, Beijing, China.

### *3.4. Prep-HPLC Analysis*

Aliquots (10 mg/mL) of freeze-dried samples resolved in $H_2O$ (Analytical grade, Merck KGaA, Darmstadt, Germany) were centrifuged at 12,000 rpm for 20 min. The supernatant was filtered through 0.22 μm membrane (Sangon, Shanghai, China), and the filtration was collected for further analysis. Prep-HPLC was run using Waters 2707 (Waters, Milford, Massachusetts, USA) linked with UPLC Sunfire C18 column (5 μm, 10 × 250 mm) (Waters, Massachusetts, USA) at the following parameters: column temperature, 40 °C; injection volume, 100 μL; and mobile phase of methanol (eluent A) and water (eluent B) at a flow rate of 4 mL/min (isocratic elution: 0–15 min, 20% eluent A and 80% eluent B). Photo-diode array (PDA) spectra were measured in the wavelength ranging from 200 to 600 nm.

### *3.5. UHPLC–MS Analysis*

The UHPLC–MS analysis was carried out using EXIONLC System (Sciex, Framingham, MA, USA) by Shanghai Hoogen Biotech, Shanghai, China using the parameters as described previously [31]. The mobile phase A contained 0.1% formic acid in $H_2O$ (*v/v*), and mobile phase B was acetonitrile (Merck KGaA, Darmstadt, Germany); column temperature: 40 °C; auto-sampler temperature: 4 °C; injection volume: 2 μL. Typical ion source parameters were: IonSpray voltage: +5500/−4500 V; curtain gas: 35 psi; temperature: 400 °C; ion source Gas 1:60 psi; ion source Gas 2: 60 psi; and declustering potential (DP): ±100 V. The SCIEX Analyst Work Station Software (Version 1.6.3) was employed for multiple reaction monitoring (MRM) data acquisition and processing. In-house R program and database were applied for peak detection and annotation (Shanghai Hoogen Biotech, Shanghai, China).

### *3.6. Transmission Electron Microscope (TEM) Assay*

Samples for TEM analysis were prepared according to the method described previously [32]. Briefly, 1 × MIC concentration of CC 1 from *R. madaio* Makino was added in bacterial culture (5 mL) at middle logarithmic growth phase (mid-LQP), and incubated at 37 °C for 2 h, 4 h and 6 h, respectively. A 1.5 mL of the cell suspension were collected, washed, fixed, and observed using SU5000 transmission electron microscope (Hitachi, Tokyo, Japan, 5.0 kV, ×30,000) [32].

### *3.7. Bacterial Cell Surface Hydrophobicity, Membrane Fluidity and Damage Assays*

Bacterial cell surface hydrophobicity and membrane fluidity were measured according to the methods by Krausova et al. [33] and Kuhry et al. [34], respectively. In the former method, 1 mL of 98% cetane (Sangon, Shanghai, China) was added into 1 mL of bacterial cell suspension ($OD_{600\,nm}$ values of 0.55 to 0.60) and rotated for 1 min and then stood at room temperature for 30 min. The absorbance of the aqueous phase was measured at

$OD_{600\,nm}$ using BioTek Synergy 2 (BioTek, Burlington, VT, USA). To measure the membrane fluidity, a 200 μL/well of bacterial suspension was mixed with 2 μL of 10 mM 1,6-diphenyl-1,3,5-hexatriene (DPH) (Sangon, China), and the change of fluorescence intensity of each well was measured at excitation light wavelength of 362 nm and emission light wavelength of 427 nm using BioTek Synergy 2 (BioTek, Burlington, VT, USA).

Cell membrane damage was examined according to the method described previously [32]. Briefly, the bacterial cell suspension was double-dyed using propidium iodide (PI, 10 mM final concentration) (Sangon, China), and 5(6)-carboxydiacetate fluorescein succinimidyl ester (CFDA, 10 mM final concentration) (Beijing Solarbio Science & Technology Co. Ltd., Beijing, China), and determined using Flow Cytometer BD FACSVerse™ (Becton, Dickinson and Company, Franklin Lakes, NJ, USA) [32].

### *3.8. Cell Membrane Permeability Analysis*

Bacterial culture at the mid-LGS was mixed with 1 × MIC concentration of the CC 1 from *R. madaio* Makino and then incubated at 37 °C for 2 h, 4 h and 6 h. Outer membrane permeability was measured according to the method described previously [35]. Briefly, a 200 μL/well of bacterial cell suspension was mixed with 2 μL/well of 10 mm NPN solution (Sangon, Shanghai, China). The excitation and emission wavelengths were set at 350 nm and 420 nm, respectively, and recorded using BioTek Synergy 2 (BioTek, Burlington, VT, USA) [35].

Inner membrane permeability was measured according to the method described previously [36]. Briefly, a 200 μL/well of bacterial cell suspension was mixed with 2.5 μL/well of 10 mm ONPG solution (Sangon, Shanghai, China). The cell mixture was incubated at 37 °C and measured for each well at $OD_{415\,nm}$ using BioTek Synergy 2 (BioTek, Burlington, VT, USA) every 30 min for 5 h, which was marked as $OD_1$, while $OD_2$ generated from the untreated bacterial suspension was used as a negative control [36].

### *3.9. Illumina RNA Sequencing*

Bacterial culture at the mid-LGP was treated with 1 × MIC concentration of the CC 1 from *R. madaio* Makino for 6 h. Total RNA was prepared using RNeasy Protect Bacteria Mini Kit (QIAGEN Biotech Co. Ltd., Frankfurt, Germany) and QIAGEN RNeasy Mini Kit (QIAGEN). DNA was removed from the samples using RNase-Free DNase Set (QIAGEN). Three independently prepared RNA samples were used for each Illumina RNA-sequencing analysis. Illumina sequencing was conducted by Shanghai Majorbio Bio-pharm Technology Co. Ltd. (Shanghai, China) using Illumina HiSeq 2500 platform (Illumina, Santiago, CA, USA). High quality reads that passed the Illumina quality filters were used for sequence analyses [32].

### *3.10. Reverse Transcription Real Time-Quantitative PCR (RT-qPCR) Assay*

Total RNA extraction, reverse transcription reactions, and relative quantitative PCR reactions were performed using the same kits and instrument according to the method described previously [31]. The 16S rRNA gene was used as the internal reference gene, and $2^{-\Delta\Delta Ct}$ method was used to calculate relative expression of genes. Oligonucleotide primers used for the RT-qPCR were synthesized by Sangon, Shanghai, China.

### *3.11. Data Analysis*

Expression of each gene was calculated using RNA-Seq by Expectation-Maximization (RSEM, http://deweylab.github.io/RSEM/, accessed on 17 October 2021). Genes with the criteria, fold-changes $\geq$ 2.0 or $\leq$0.5, and $p$-values < 0.05 relative to the control were defined as DEGs. These DEGs were used for gene set enrichment analysis (GSEA) against the Kyoto Encyclopedia of Genes and Genomes (KEGG) database (https://www.genome.jp/kegg/, accessed on 17 October 2021). Significantly changed GSEA were identified when the enrichment test $p$-value fell below 0.05 [32]. All tests were performed in triplicates. The

data were analyzed using SPSS statistical analysis software version 17.0 (SPSS Inc., Armonk, NY, USA).

## 4. Conclusions

In this study, we identified, for the first time, antibacterial components and action modes of methanol-phase extract from one edible herbaceous plant *R. madaio* Makino. The bacteriostatic rate of the extract was 75% against 23 species of common pathogenic bacteria, which was higher than that of the chloroform-phase extract (39%). The methanol-phase extract was further purified using the Prep-HPLC technique, and five separated CCs were obtained. Among these, the CC 1 from *R. madaio* Makino significantly increased bacterial cell surface hydrophobicity and membrane permeability and decreased membrane fluidity of Gram-positive and Gram-negative pathogens, such as *V. parahaemolyticus* ATCC17802, *V. parahaemolyticus* B4-10, *V. alginolyticus* ATCC17749, and *B. cereus* A1-1. The damaged cell surface and membrane structure integrity facilitated the CC1 to penetrate bacterial cell envelope to target intracellular processes. A total of 58 different compounds in the extract were identified using UHPLC–MS technique. Comparative transcriptomic analyses revealed a number of differentially expressed genes (DGEs) and various changed metabolic pathways mediated by the CC1 action, such as down-regulation of carbohydrate transport and/or utilization, and energy metabolism; upward regulation of amino acid and fatty acid degradation, and nitrogen metabolism; and inactive flagellar assembly and mobility in the four bacterial strains. Taken, the results in this study demonstrated that the CC1 from *R. madaio* Makino are promising candidates for antibacterial medicine and human health care products.

**Supplementary Materials:** The following supporting information can be downloaded at. Table S1: Bacterial strains and media used in this study; Table S2: Expression of representative DEGs by RT-qPCR assay.

**Author Contributions:** Y.L.: investigation, data curation, and writing—original draft preparation; L.Y.: data analysis; P.L.: assistance in the instrument for the extract preparation; Y.J.: discussion; S.Q.: supervision, and discussion; L.C.: funding acquisition, conceptualization, and writing—review and editing. All authors have read and agreed to the published version of the manuscript.

**Funding:** This study was supported by Shanghai Municipal Science and Technology Commission, grant number 17050502200, and National Natural Science Foundation of China, grant number 31671946.

**Institutional Review Board Statement:** Not applicable.

**Informed Consent Statement:** Not applicable.

**Data Availability Statement:** A complete list of DEGs in the four strains were available in the NCBI SRA database (https://submit.ncbi.nlm.nih.gov/subs/bioproject/, accessed on 17 October 2021) under the accession number PRJNA767551.

**Acknowledgments:** The authors are grateful to Yaping Wang and Ling Ni for their help in the extract preparation and to Zhengke Shen for her assistance in the manuscript preparation.

**Conflicts of Interest:** The authors declare no conflict of interest.

**Sample Availability:** Samples of the methanol-phase extract from *R. malaio* Makino are available from the authors by request.

## References

1. Huang, J.; Huang, J.; Lu, X.; Ma, K. Diversity distribution patterns of Chinese endemic seed plant species and their implications for conservation planning. *Sci. Rep.* **2016**, *6*, 33913. [CrossRef] [PubMed]
2. Xu, X.; Xu, H.; Shang, Y.; Zhu, R.; Hong, X.; Song, Z.; Yang, Z. Development of the general chapters of the Chinese Pharmacopoeia 2020 edition: A review. *J. Pharm. Anal.* **2021**, *11*, 398–404. [CrossRef] [PubMed]
3. Ye, Y.; Xia, M.; Mu, C.; Li, R.; Wang, C. Acute metabolic response of *Portunus trituberculatus* to *Vibrio alginolyticus* infection. *Aquaculture* **2016**, *463*, 201–208. [CrossRef]

4. Lv, T.; Song, T.; Liu, H.; Peng, R.; Jiang, X.; Zhang, W.; Han, Q. Isolation and characterization of a virulence related *Vibrio alginolyticus* strain Wz11 pathogenic to Cuttlefish, Sepia pharaonis. *Microb. Pathog.* **2019**, *126*, 165–171. [CrossRef]
5. Li, L.; Meng, H.; Gu, D.; Li, Y.; Jia, M. Molecular mechanisms of *Vibrio parahaemolyticus* pathogenesis. *Microbiol. Res.* **2019**, *222*, 43–51. [CrossRef]
6. Bottone, E.J. *Bacillus cereus*, a volatile human pathogen. *Clin. Microbiol. Rev.* **2010**, *23*, 382–398. [CrossRef]
7. Danchik, C.; Casadevall, A. Role of cell surface hydrophobicity in the pathogenesis of medically-significant fungi. *Front. Cell. Infect. Microbiol.* **2020**, *10*, 594973. [CrossRef] [PubMed]
8. Ma, S.; Ding, L.; Hu, H.; Ma, H.; Xu, K.; Huang, H.; Geng, J.; Ren, H. Cell membrane characteristics and microbial population distribution of MBBR and IFAS with different dissolved oxygen concentration. *Bioresour. Technol.* **2018**, *265*, 17–24. [CrossRef] [PubMed]
9. Aqawi, M.; Sionov, R.V.; Gallily, R.; Friedman, M.; Steinberg, D. Anti-bacterial properties of cannabigerol toward *Streptococcus mutans*. *Front. Microbiol.* **2021**, *12*, 656471. [CrossRef] [PubMed]
10. Bajpai, V.K.; Sharma, A.; Baek, K.-H. Antibacterial mode of action of *Ginkgo biloba* leaf essential oil: Effect on morphology and membrane permeability. *Bangl. J. Pharmacol.* **2015**, *10*, 337. [CrossRef]
11. Zhang, D.; Nie, S.; Xie, M.; Hu, J. Antioxidant and antibacterial capabilities of phenolic compounds and organic acids from *Camellia oleifera* cake. *Food Sci. Biotechnol.* **2020**, *29*, 17–25. [CrossRef]
12. Cushnie, T.P.T.; Cushnie, B.; Lamb, A.J. Alkaloids: An overview of their antibacterial, antibiotic-enhancing and antivirulence activities. *Int. J. Antimicrob. Agents* **2014**, *44*, 377–386. [CrossRef] [PubMed]
13. Kumari, A.; Singh, R.K. Medicinal chemistry of indole derivatives: Current to future therapeutic prospectives. *Bioorg. Chem.* **2019**, *89*, 103021. [CrossRef] [PubMed]
14. Wang, M.; Wu, J.; Wu, D. Cloning and expression of the sucrose phosphorylase gene in *Bacillus* subtilis and synthesis of kojibiose using the recombinant enzyme. *Microb. Cell Fact.* **2018**, *17*, 23. [CrossRef]
15. Garcia, C.A.; Gardner, J.G. Bacterial α-diglucoside metabolism: Perspectives and potential for biotechnology and biomedicine. *Appl. Microbiol. Biotechnol.* **2021**, *105*, 4033–4052. [CrossRef] [PubMed]
16. Jarzyniak, K.; Banasiak, J.; Jamruszka, T.; Pawela, A.; Di Donato, M.; Novák, O.; Geisler, M.; Jasiński, M. Early stages of legume-rhizobia symbiosis are controlled by ABCG-mediated transport of active cytokinins. *Nat. Plants* **2021**, *7*, 428–436. [CrossRef] [PubMed]
17. Tsao, S.; Rahkhoodaee, F.; Raymond, M. Relative contributions of the *Candida albicans* ABC transporters Cdr1p and Cdr2p to clinical azole resistance. *Antimicrob. Agents Chemother.* **2009**, *53*, 1344–1352. [CrossRef] [PubMed]
18. Tarling, E.J.; de Aguiar Vallim, T.Q.; Edwards, P.A. Role of ABC transporters in lipid transport and human disease. *Trends Endocrinol. Metab.* **2013**, *24*, 342–350. [CrossRef]
19. Whitley, M.J.; Arjunan, P.; Nemeria, N.S.; Korotchkina, L.G.; Park, Y.H.; Patel, M.S.; Jordan, F.; Furey, W. Pyruvate dehydrogenase complex deficiency is linked to regulatory loop disorder in the αV138M variant of human pyruvate dehydrogenase. *J. Biol. Chem.* **2018**, *293*, 13204–13213. [CrossRef]
20. Aquilano, K.; Vigilanza, P.; Rotilio, G.; Ciriolo, M.R. Mitochondrial damage due to SOD1 deficiency in SH-SY5Y neuroblastoma cells: A rationale for the redundancy of SOD1. *FASEB J.* **2006**, *20*, 1683–1685. [CrossRef]
21. Hajam, I.A.; Dar, P.A.; Shahnawaz, I.; Jaume, J.C.; Lee, J.H. Bacterial flagellin-a potent immunomodulatory agent. *Exp. Mol. Med.* **2017**, *49*, e373. [CrossRef]
22. Nedeljković, M.; Sastre, D.E.; Sundberg, E.J. Bacterial flagellar filament: A supramolecular multifunctional nanostructure. *Int. J. Mol. Sci.* **2021**, *22*, 7521. [CrossRef] [PubMed]
23. Carroll, B.L.; Nishikino, T.; Guo, W.; Zhu, S.; Kojima, S.; Homma, M.; Liu, J. The flagellar motor of *Vibrio alginolyticus* undergoes major structural remodeling during rotational switching. *Elife* **2020**, *9*. [CrossRef] [PubMed]
24. Ahmad, F.; Zhu, D.; Sun, J. Bacterial chemotaxis: A way forward to aromatic compounds biodegradation. *Environ. Sci. Eur.* **2020**, *32*, 52. [CrossRef]
25. LeBlanc, M.A.; Fink, M.R.; Perkins, T.T.; Sousa, M.C. Type III secretion system effector proteins are mechanically labile. *Proc. Natl. Acad. Sci. USA* **2021**, *118*. [CrossRef] [PubMed]
26. van den Berg, W.A.; Hagen, W.R.; van Dongen, W.M. The hybrid-cluster protein ('prismane protein') from *Escherichia coli*. Characterization of the hybrid-cluster protein, redox properties of the [2Fe-2S] and [4Fe-2S-2O] clusters and identification of an associated NADH oxidoreductase containing FAD and [2Fe-2S]. *Eur. J. Biochem.* **2000**, *267*, 666–676. [CrossRef]
27. Xue, M.; Raheem, M.A.; Gu, Y.; Lu, H.; Song, X.; Tu, J.; Xue, T.; Qi, K. The KdpD/KdpE two-component system contributes to the motility and virulence of avian pathogenic *Escherichia coli*. *Res. Vet. Sci.* **2020**, *131*, 24–30. [CrossRef]
28. Xu, M.; Fu, H.; Chen, D.; Shao, Z.; Zhu, J.; Alali, W.Q.; Chen, L. Simple visualized detection method of virulence-associated genes of *Vibrio cholerae* by loop-mediated isothermal amplification. *Front. Microbiol.* **2019**, *10*, 2899. [CrossRef] [PubMed]
29. Wang, Y.; Chen, L.; Pandak, W.M.; Heuman, D.; Hylemon, P.B.; Ren, S. High glucose Induces lipid accumulation via 25-Hydroxycholesterol DNA-CpG methylation. *iScience* **2020**, *23*, 101102. [CrossRef]
30. Chen, D.; Li, X.; Ni, L.; Xu, D.; Xu, Y.; Ding, Y.; Xie, L.; Chen, L. First experimental evidence for the presence of potentially toxic *Vibrio cholerae* in *Snails*, and virulence, cross-resistance and genetic diversity of the bacterium in 36 species of aquatic food animals. *J. Antibiot.* **2021**, *10*, 412. [CrossRef]

31. Shan, X.; Fu, J.; Li, X.; Peng, X.; Chen, L. Comparative proteomics and secretomics revealed virulence, and coresistance-related factors in non O1/O139 *Vibrio cholerae* recovered from 16 species of consumable aquatic animals. *J. Proteom.* **2021**, *251*, 104408. [CrossRef] [PubMed]
32. Yang, L.; Wang, Y.; Yu, P.; Ren, S.; Zhu, Z.; Jin, Y.; Yan, J.; Peng, X.; Chen, L. Prophage-related gene *VpaChn25_0724* contributes to cell membrane Integrity and growth of *Vibrio parahaemolyticus* CHN25. *Front. Cell. Infect. Microbiol.* **2020**, *10*, 595709. [CrossRef] [PubMed]
33. Krausova, G.; Hyrslova, I.; Hynstova, I. In vitro evaluation of adhesion capacity, hydrophobicity, and auto-aggregation of newly isolated potential probiotic strains. *Fermentation* **2019**, *5*, 100. [CrossRef]
34. Kuhry, J.G.; Duportail, G.; Bronner, C.; Laustriat, G. Plasma membrane fluidity measurements on whole living cells by fluorescence anisotropy of trimethylammoniumdiphenylhexatriene. *Biochim. Biophys Acta.* **1985**, *845*, 60–67. [CrossRef]
35. Wang, Z.; Qin, Q.; Zheng, Y.; Li, F.; Zhao, Y.; Chen, G.-Q. Engineering the permeability of *Halomonas bluephagenesis* enhanced its chassis properties. *Metab. Eng.* **2021**, *67*, 53–66. [CrossRef] [PubMed]
36. Huang, B.; Liu, X.; Li, Z.; Zheng, Y.; Wai Kwok Yeung, K.; Cui, Z.; Liang, Y.; Zhu, S.; Wu, S. Rapid bacteria capturing and killing by AgNPs/N-CD@ZnO hybrids strengthened photo-responsive xerogel for rapid healing of bacteria-infected wounds. *Chem. Eng. J.* **2021**, *414*, 128805. [CrossRef]